Interfacial Electro-Thermal Runaway Dynamics in Medium Voltage AC Conductor Sleeves

Doctoral Thesis

by

RITESH KUMAR 2018EEZ0013



DEPARTMENT OF ELECTRICAL ENGINEERING INDIAN INSTITUTE OF TECHNOLOGY ROPAR JUNE 2025

Interfacial Electro-Thermal Runaway Dynamics in Medium Voltage AC Conductor Sleeves

A Thesis Submitted

In Partial Fulfilment of the Requirements

for the Degree of

DOCTOR OF PHILOSOPHY

by

RITESH KUMAR 2018EEZ0013



DEPARTMENT OF ELECTRICAL ENGINEERING INDIAN INSTITUTE OF TECHNOLOGY ROPAR

JUNE 2025

Ritesh Kumar: Interfacial <i>electro thermal runaway dynamics in medium voltage AC conductor sleeves</i> Copyright © 2025, Indian Institute of Technology Ropar All Rights Reserved	

Dedicated to Family

I dedicate this thesis to my parents, my wife, my daughter, and my in-laws. I am profoundly grateful to my parents for believing in me and for their unwavering support throughout my academic journey. A special note of appreciation goes to my wife, whose encouragement and financial support have been instrumental in my success, and to my daughter, whose presence has been a source of immense joy and motivation. I am also deeply thankful to my in-laws for their steadfast support and understanding. Each of you has been a driving force in my Ph.D. journey, and I look forward to your continued support in all my future endeavours.

Declaration of Originality

I hereby declare that the work, which is being presented in the thesis entitled "Interfacial Electro Thermal Runaway Dynamics in Medium Voltage AC Conductor Sleeves", has been solely authored by me. It presents the result of my own independent investigation/research conducted during the time period from July 2018 to June 2025 under the supervision of Prof. C.C. Reddy, IIT Ropar. To the best of my knowledge, it is an original work, both in terms of research content and narrative, and has not been submitted or accepted elsewhere, in part or in full, for the award of any degree, diploma, fellowship, associateship, or similar title of any university or institution. Further, due credit has been attributed to the relevant state-of-the-art and collaborations (if any) with appropriate citations and acknowledgments, in line with established ethical norms and practices. I also declare that any idea/data/fact/source stated in my thesis has not been fabricated/ falsified/ misrepresented. All the principles of academic honesty and integrity have been followed. I fully understand that if the thesis is found to be unoriginal, fabricated, or plagiarized, the Institute reserves the right to withdraw the thesis from its archive and revoke the associated Degree conferred. Additionally, the Institute also reserves the right to appraise all concerned sections of society of the matter for their information and necessary action (if any). If accepted, I hereby consent for my thesis to be available online in the Institute's Open Access repository, inter-library loan, and the title & abstract to be made available to outside organizations.

Signature

Name: RITESH KUMAR

Ritesh Kumar

Entry Number: 2018EEZ0013

Program: PhD. Department: EED

Indian Institute of Technology Ropar

Rupnagar, Punjab 140001

Date: 19/6/25

Acknowledgments

I wish to thank my supervisor Prof. C. C. Reddy for the continuous support and encouragement throughout my journey as a PhD candidate. I am inspired by his knowledge and problem-solving skills. I wish to continue on his path to share my knowledge with others.

I am also immensely thankful to the IIT Ropar for giving me the opportunity to pursue my professional degree. I extend my gratitude to the Chairman Dr. Subramanya Murala for his valuable guidance and support. I am deeply appreciative to the doctoral committee members Dr. Saifullah Payami, Dr. Kalaiselvi J., and Dr. Subash Chandra Martha for their constructive direction and timely support

Thanks to my respectful seniors Dr. Alam Pratap Singh, Dr. Avnish Kumar, Dr. Ajit John Thomss, Dr. Satyamoorthy and Dr. Birender Singh for sharing their knowledge, as well as thankful to my former colleagues Dr. Priyesh kumar pandey and Dr. Iyyapan C for their valuable technical discussions. To my present colleagues - Purna, Pranav, Aritra, Harshith, Parimal, Anas, Akshay, Prity, Amit, and Subham, I am grateful for your continuous support.

Finally, I extend my heartfelt thanks to Mr. Dilbag Singh and Mr. Jaspreet Singh for their continuous assistance throughout my research journey in laboratory experiments.

Certificate

This is to certify that the thesis entitled "Interfacial Electro Thermal Runaway Dynamics in Medium Voltage AC Conductor Sleeves" submitted by RITESH KUMAR (2018EEZ0013) for the award of the degree of Doctor of Philosophy of Indian Institute of Technology Ropar, is a record of genuine research work carried out under my (our) guidance and supervision. To the best of my knowledge the work presented in this thesis is original and has not been submitted to anywhere for any purpose of award of degree.

Signature of the Supervisor

Prof. C.C. Reddy

Electrical Engineering Department

Indian Institute of Technology Ropar

Rupnagar, Punjab 140001

Lay Summary

Insulation is a critical component in ensuring the efficiency and longevity of power equipment. The type of insulation material used depends on the application; for example, kraft paper is commonly employed in transformers, while polymers are integral to power cables, covered conductors (CCs), and conductor sleeves (CS). The reliability and service life of electrical equipment are largely determined by the quality and performance of its insulation. In high-voltage systems, specialized testing methods are used to assess insulation behavior under operational stresses, guiding the design of tailored solutions.

This thesis focuses on the electro-thermal performance and reliability of CS in medium-voltage transmission networks. CS offer significant benefits over bare and covered conductors, such as enhanced flexibility, improved safety, and reduced maintenance requirements. Despite these advantages, CS are prone to electrical stresses like tracking and electro-thermal instability, which can lead to insulation failure and shorten their operational lifespan.

Through a combination of experimental investigations and simulations, the study examines the performance of two CS configurations; 90° and 180° overlapped and compared their outcomes with CCs. Novel testing setups are developed and used to measure surface and interfacial conductivity, while Finite Element Modelling (FEM) evaluates their response under extreme conditions, such as tree branch contact with the CS surface.

The findings reveal that 180° overlapping sleeves provide superior insulation performance and stability compared to the 90° configuration. The research recommends increasing the insulation thickness of 90° sleeves to enhance their performance.

The thesis proposes a work that contributes to optimizing conductor sleeve designs, enabling safer and more efficient power transmission while minimizing risks associated with environmental and operational stresses.

Abstract

Introduction: Tracking and electro-thermal runaway are critical failure mechanisms in overhead conductor sleeves that compromise the safety and reliability of power transmission systems. The geometric configuration of sleeve overlaps plays a significant role in determining susceptibility to these phenomena. This study investigates the influence of 90° and 180° overlap configurations on the initiation and progression of electrical tracking and thermal runaway under alternating current (AC) stress.

Methodology: A combined experimental and simulation-based approach was employed. A novel experimental setup was developed to measure surface and interfacial conductivity of sleeve materials under varying thermal and electrical conditions. Interface Tracking Inception Voltage (ITIV) was evaluated for both configurations. Additionally, Finite Element Method (FEM)-based simulations were conducted to model electro-thermal behavior, incorporating the dependency of conductivity on temperature and electric field.

Results: Experimental findings revealed that the 90° overlap configuration exhibited earlier tracking onset and higher susceptibility to thermal runaway compared to the 180° configuration. The ITIV was consistently lower for 90° overlaps. Simulation results supported the experimental observations, showing greater thermal and electrical stress concentration in 90° overlaps. Comparative analysis with traditional covered conductors (CCs) and conductor sleeves (CS) confirmed the advantages of optimized overlap designs.

Discussion: The study highlights the critical role of overlap geometry in improving the performance of overhead conductor sleeves. The 180° configuration demonstrated superior stability, reduced tracking events, and better resistance to electro-thermal degradation. These insights offer practical recommendations for enhancing the design of conductor sleeves, with direct implications for improving reliability and reducing the maintenance costs of power transmission infrastructure.

Keywords: Conductor sleeve, covered conductor, AC conductivity, surface and interface current measurement, dielectric measurement, electrical tracking, insulation degradation and electro-thermal runaway.

List of Publications

Patents

 R Kumar, Pranav Johri, A Harshith Kumar, and C. C. Reddy "A method and system for optimizing conductor sleeves design through AC conductivity measurement", Indian Patent, Application No: 202411065987 (Published)

Journals

- R. Kumar and C. C. Reddy, "Assessment of Electro-Thermal Runaway Dynamics of AC Conductor Sleeves Designed for Medium Voltage Transmission System," in *IEEE Transactions on Dielectrics and Electrical Insulation*, doi: 10.1109/TDEI.2024.3484371.
- **2.** R. Kumar and C. C. Reddy "Impact on load current on the insulation integrity of Conductor sleeves insulated conductor used in medium voltage transmission system" (To be submitted in TDEIS).

Conferences

- R. Kumar, P. Johri, P. Sharma and C. C. Reddy, "AC Conductivity Measurement of Conductor Sleeves" 2024 IEEE 7th International Conference on Condition Assessment Techniques in Electrical Systems (CATCON), Jadavpur University, India.
- 2. P. Sharma, R. Kumar and C. C. Reddy, "Investigation on Cable Breakdown Using Aluminium Foil as Electrode" 2024 IEEE 7th International Conference on Condition Assessment Techniques in Electrical Systems India

Table of Contents

Declaration of Originality	5
Acknowledgments	6
Certificate	7
Lay summary	8
Abstract	9
List of publications	10
Table of contents	11
List of Figures	13
List of Tables	16
Notations and Abbreviations	17
Chapter 1 Introduction	18
1.1 Brief overview of overhead transmission lines	18
1.2 Covered conductors	21
1.2.1 Conductor sleeves	25
1.3 Conclusions	25
Chapter 2 Literature survey	26
2.1 Electrical tracking and thermal runaway in covered conductors	26
2.2 Mitigation strategy for electrical tracking	30
2.3 Partial discharge in covered conductors	30
2.4 Fault conditions in covered conductors	31
2.4.1 Causes of fault in covered conductors	31
2.4.2 Protective measure & fault tolerant design	32
2.4.3 Limitations of covered conductors	33
2.5 Conductor sleeves in medium voltage system	33
2.5.1 Application of conductor sleeves in medium voltage system	34
2.6 Motivation	34

2.7 Problem statement	35
2.8 Applicability of covered conductor and conductor sleeve across voltage lev	el36
2.9 Chapter wise contribution to the thesis	38
2.10 Conclusions	40
Chapter 3 AC conductivity measurement	41
3.1 AC volumetric current measurement	41
3.2 Surface current measurement	43
3.3 Interface current measurement	50
3.4 Analysis of conductivity variations and their implications	53
3.5 Conclusions	54
Chapter 4 FEM Modelling, analysis and validation of conductor sleeves performa	ance55
4.1 Geometry, material properties & simulation model	55
4.2 Governing equation	56
4.3 Analysis & interpretation of simulation results	58
4.4 Analysis & validation of tracking inception voltage in insulated conductor s	ystem68
4.5 Limitation of simulation model and discrepancy analysis	71
4.6 Conclusions	71
Chapter 5 Impact of load current performance of conductor sleeves	
5.1 CS without insulation tape	
5.2 CS with insulation tape	76
5.3 FEM based analysis of load current effects on runaway phenomenon	
5.4 Conclusions	80
Chapter 6 Conclusion and future work	81
6.1 Conclusions	
6.2 Future work	
References	

List of Figures

Figure 1.1 Bird and Animal Electrocution and Fire Risk [1]	19
Figure 1.2 Structural Design of Covered Conductors for Overhead Power Lines	22
Figure 1.3. Voltage distribution of Covered conductor [5]	23
Figure 2.1 Process of electrical tracking rupture in humid environments [6]	28
Figure 2.2 Semiconducting tube placed on CC to investigate tracking [13]	29
Figure 2.3 Example of a high-impedance fault occurs when tree branches come into contact with overhead CCs [26]	31
Figure 2.4 Medium voltage AC conductor sleeves: (a) Cross sectional view of CS (b) Implementation of CS on Transmission Systems	35
Figure 3.1 Silicon rubber-based CS (a) 180° overlapping angle (b) 90° overlapping angle configuration	41
Figure 3.2 Volumetric ac conductivity of CS with respect to temperature and electric field: experimental and curve-fitted	43
Figure 3.3 Schematic diagram for surface current measurement on CS	44
Figure 3.4 Experimental setup for surface current measurement (inside oven view)	45
Figure 3.5. (a) Representation of equivalent circuit of dielectric (b) equivalent circuit of proposed setup	46
Figure 3.6 Measured voltage at 1 kV at 303.15 K	47
Figure 3.7 Surface conductivity of CS with respect to temperature and electric field:	40
experimental and curve-fitted	49
Figure 3.8 Schematic diagram for interface current measurement.	50
Figure 3.9 Experimental setup for interface current measurement (b) measuring setup (inside oven view)	51
Figure 3.10 Interfacial ac conductivity of CS with respect to temperature and field: experimental and curve-fitted	51

configuration	55
Figure 4.2 Electric field distribution at rated voltage for (a) 180° overlapped (b) 90°	59
overlapped configuration	
Figure 4.3 Enlarged view of selected area of figure 4.2	59
Figure 4.4 Current density distribution at rated voltage for (a) 180° overlapped (b) 90° overlapped configuration	60
Figure 4.5 Electric field distribution at rated voltage, in case of tree branch touching the CS surface for (a) 180° overlapped (b) 90° overlapped configuration	60
Figure 4.6 Current density distribution at rated voltage, in case of tree branch touching the	
CS surface for (a) 180° overlapped (b) 90° overlapped configuration	61
Figure 4.7 (a) Peak electric field and (b) current density relative to ground electrode distance from CS surface	61
Figure 4.8 Runaway in 180° CS (a) Electric field (b) Temperature and (c) Temperature Distribution	63
Figure 4.9 Runaway in 90° CS (a) Electric field (b) Temperature and (c) Field Distribution	63
Figure 4.10 Equipotential line distribution in 180°CS for (a) 5mm and (b) 1mm distance from surface	64
Figure 4.11 V-t characteristics for 5 mm ground electrode distance from CS surface	65
Figure 4.12 V-t characteristics for 2.5 mm ground electrode distance from CS surface	65
Figure 4.13 V-t characteristics for 1 mm ground electrode distance from CS surface	66
Figure 4.14 V-t characteristics for ground electrode at 5mm, 2.5mm, and 1mm from CS surface	66
Figure 4.15 Electric field distribution at rated voltage in the (a) CC (b) 90° overlapped CS (c) 180° overlapped CS	67
Figure 4.16 $\mathrm{ITIV}_{\mathrm{Sim}}$ Vs. insulation thickness for CC, 90° and 180° overlapped CS	68
Figure 4.17 Evperimental setup for estimation of ITM	66
Figure 4.17 Experimental setup for estimation of ITIV	69
Figure 4.18 (a) $ITIV_{Exp}$ Characteristics of CC and CS and (b) Surface tracking path formation	69
Figure 5.1 Schematic representation of experimental setup for electrical tracking	7/

phenomena under varying loading conditions.

Figure 5.2 Experimental setup for electrical tracking phenomena under varying loading	_
conditions	75
Figure 5.3 Conductor sleeve when insulation tape applied on the outer tip of interfacial	_
region.	76
Figure 5.4 Schematic representation of experimental setup for electrical tracking	_,
phenomena under varying loading conditions with insulation tape.	78
Figure 5.5 Experimentally obtained interfacial tracking inception voltage with and without	_,
insulation tape	78
Figure 5.6 Runaway characteristics in the interface region for 180° (90° initial temperature)	
overlapped CS.	79

List of Tables

Table 3.1 Estimated coefficients & goodness of fit statistics	43
Table 3.2 Measured surface AC resistivity & conductivity for different applied voltage and Temperatures	48
Table 3.3 Estimated surface coefficients of CS & goodness of fitting	49
Table 3.4 Estimated interfacial coefficients of CS & goodness of fitting	52
Table 3.5 Measured interfacial AC resistivity & conductivity for different voltages and temperatures	52
Table 3.6 Estimated volumetric conductivity of bulk, surface and in the interface of CS	53
Table 4.1 Simulation model parameters	56
Table 4.2 Peak electric field & current density in the interface of CS at rated voltages	62
Table 4.3 Comparison of tracking inception voltage with the runaway inception voltage in the interface of CS & CC surface	69
Table 5.1 Load current & thermal effects on conductor sleeve performance without insulation tape	75
Table 5.2 Load current & thermal effects on conductor sleeve performance with insulation tape	77

Notations and Abbreviations

CCs	Covered conductors	T	Temperature in K
σ_{AC}	AC conductivity	R_{m}	Measuring Resistance
$oldsymbol{arepsilon}^*$	Complex permittivity	OBC	Overhead bare conductor
$oldsymbol{arepsilon}'$	Real part of permittivity	A	Conductivity coefficients(S/m)
$oldsymbol{arepsilon}^{\prime\prime}$	Imaginary part of permittivity	PD	Partial discharge
UV	Ultraviolet	α	Electric field coefficients(m/v)
EPR	Ethylene propylene rubber	β	Temperature coefficient(K)
Tan δ	Dissipation factor	$ ho_s$	Surface resistivity
TDR	Time domain reflectometry	FEM	Finite element method
UHF	Ultra-high frequency	HV	High voltage
Si-R	Silicon rubber	MV	Medium voltage
CS	Conductor sleeves	P	Perimeter(mm)
σ_{sv}	Volumetric surface conductivity(S/m)	\boldsymbol{g}	Gap between electrode(mm)
σ_{iv}	Volumetric interfacial conductivity(S/m)	XLPE	Cross linked polyethylene
$\sigma_{\rm v}$	Bulk conductivity (S/m)	SSE	Sum of squares error
Φ	Phase angle	V_z	Surface voltage
ω	Angular frequency	D	Diameter of electrode

Chapter 1 Introduction

Power transmission plays a crucial role in transferring electrical energy from generation points, such as power plants, renewable energy facilities, and substations, to various endusers, including homes, industries, and businesses. Since these generation sources are often located far from the areas where electricity is consumed, transmission systems are designed to move power efficiently over long distances while minimizing losses. This enables a consistent, stable, and economical electricity supply, commonly achieved through overhead transmission lines.

1.1 Brief overview of Overhead Transmission Lines

Overhead transmission lines play a crucial role in modern power systems by enabling the long-distance transportation of electricity from power generation plants to distribution networks. These lines consist of conductors suspended on towers or poles and operate at high voltages to minimize energy losses during transmission. The conductors are typically made of materials such as aluminum or copper, and the towers or poles provide the necessary support to keep the lines elevated above the ground. Overhead transmission lines are often chosen for their cost-effectiveness in installation and maintenance when compared to underground cables. Additionally, they are relatively easier to repair, and their construction avoids the complex and expensive underground digging processes required for cables. However, despite these advantages, overhead transmission lines are susceptible to various challenges that can lead to faults and operational disruptions.

Faults in overhead transmission lines are typically caused by factors such as extreme weather conditions, mechanical damage from external sources, and internal degradation of the components. Faults occur when there is a sudden disruption in the normal flow of electricity due to issues such as short circuits, open circuits, or ground faults. These disruptions create abnormal current paths, which can lead to equipment damage, power outages, and safety hazards. Extreme weather events, such as thunderstorms, high winds, and ice storms, can cause conductors to break or come into contact with other objects, leading to faults. Mechanical damage also plays a significant role, with fallen trees, animals, or even human activities causing conductors to touch one another or the ground, triggering faults. Internal factors, such as wear and tear of the conductors, can further exacerbate these issues.

The different types of faults that occur in overhead transmission lines include line-to-line faults, line-to-ground faults, and line-to-line-to-ground faults. A line-to-line fault occurs when two-phase conductors come into direct contact, resulting in a short circuit between them. A line-to-ground fault happens when a conductor contacts the ground, creating an abnormal current path that can damage equipment. The most severe type of fault is a line-to-line-to-ground fault, where multiple conductors simultaneously contact each other and the ground. Additionally, high impedance faults can occur when conductors partially touch nearby objects, such as vegetation, poles, or other structures. These high impedance faults are often difficult to detect and are common in areas with dense vegetation or challenging terrains like forests or mountainous regions. Though they may not cause a significant increase in current, high impedance faults can still affect system performance, leading to increased losses, reduced reliability, and grid instability.



Figure 1.1 Bird and animal electrocution and fire risk [1]

Faults in overhead transmission lines caused by tree branches touching the lines or animal activity can lead to catastrophic outcomes. In areas with dry vegetation or forests, tree branches, or even fallen trees, can come into contact with power lines. This creates an electrical path that may trigger a fault. The electrical current flowing through the tree branch can cause sparks, which, especially in dry conditions, can ignite the surrounding vegetation, leading to forest fires. These fires not only result in the destruction of vast areas of vegetation but also cause long-term damage to ecosystems and disrupt wildlife habitats. Many animals,

including birds as shown in figure 1.1, and small mammals, face the risk of death due to electrocution when they come into the direct contact with power lines, or they may perish in the fires ignited by electrical faults [1]. The loss of wildlife, particularly in areas that harbour endangered species, can have profound effects on biodiversity, leading to a decline in the health of local ecosystems.

Another major concern for overhead transmission lines is corrosion, particularly in regions where environmental conditions accelerate the degradation of metal components. Corrosion occurs when metal components, such as conductors, towers, and insulators, react with environmental elements like moisture, oxygen, and pollutants. This chemical reaction results in the gradual breakdown of metal surfaces, reducing the strength and efficiency of the components. Areas with high humidity, salty air (such as coastal regions), or air pollution are particularly susceptible to corrosion. Corrosion in conductors can weaken their mechanical strength and electrical conductivity, increasing the likelihood of failure during adverse weather conditions, such as high winds or storms. Towers and support structures are also vulnerable to corrosion, which can cause misalignment of lines, instability, or even collapse. Similarly, corrosion of insulators, which are designed to prevent the flow of electrical current to the ground, can reduce their insulating effectiveness, leading to increased leakage currents and a higher likelihood of faults.

The degradation of metal components due to corrosion can make overhead transmission lines even more prone to faults. In addition to external factors such as weather and mechanical damage, corrosion accelerates the wear and tear of components, which can lead to catastrophic failures. This highlights the importance of regular maintenance and inspection of overhead transmission lines, particularly in areas prone to corrosive environments. To counteract corrosion, operators can use protective coatings, corrosion-resistant materials, and regular inspections to ensure the longevity and reliability of transmission lines.

To mitigate the effects of faults and corrosion, utilities implement a range of preventive measures, including routine inspections, ongoing maintenance, and effective vegetation management. Regular inspections are crucial for identifying early signs of faults, corrosion, or wear, allowing for corrective actions before they cause significant damage. Vegetation management is particularly important in areas with dense tree cover or rapid plant growth. Overgrown vegetation can cause conductors to come into direct contact with trees, triggering

faults. By clearing tree branches and other vegetation along transmission lines, utilities can reduce the risk of vegetation-induced faults.

In regions prone to corrosion, utilities use protective coatings, such as specialized paints or corrosion inhibitors, to protect conductors, towers, and support structures. These coatings help prevent further degradation and ensure the longevity of transmission components. Additionally, materials that are resistant to corrosion, such as galvanized steel, stainless steel, or aluminum alloys, are increasingly used to construct towers and other components to enhance their durability. Composite insulators, which are resistant to environmental degradation, are also becoming more widely used to improve the performance and reliability of transmission lines.

To detect faults promptly, utilities deploy advanced monitoring and fault detection systems. These systems enable quick identification and isolation of faults, minimizing damage. Relay protection systems, which automatically detect abnormal current flow and disconnect affected sections of the grid, play a vital role in reducing outage durations. Real-time data acquisition systems and smart sensors offer detailed insights into the condition of overhead lines, allowing utilities to take preventive actions before faults escalate. Despite the use of various protective layers to prevent faults and corrosion in overhead transmission lines, faults remain frequent, and maintenance costs are high. Environmental factors such as extreme weather, moisture, and pollution continue to accelerate wear and tear, while wildlife interference and aging infrastructure also contribute to frequent failures.

1.2 Covered Conductors

The rapid advancement of power transmission systems has introduced covered conductors (CCs) to a revolutionary solution to address the challenges faced by overhead transmission lines as discussed in the previous section. The concept of CCs is simple yet effective design. The design of CCs is made of conductors and insulating layers as shown in figure 1.2, the conductors consist of materials like copper or aluminum, which are responsible for conducting electrical current. This central conductor is enveloped in a protective insulating made from high-performance materials such as cross-linked polyethylene (XLPE) or ethylene propylene rubber (EPR) [2].



Figure 1.2 Structural design of covered conductors for overhead power lines

The insulation provides multiple advantages by safeguarding the conductor against a variety of environmental challenges and external threats. It serves as a shield against ultraviolet (UV) radiation, moisture, and extreme temperature variations, all of which can cause traditional bare conductors to degrade and fail over time [3].

One of the primary benefits of CCs is their ability to prevent direct contact between the power line and external elements, particularly in areas where vegetation and wildlife are prevalent. Overhead transmission lines, particularly bare conductors, are highly susceptible to damage from tree branches, falling debris, or wildlife interference. Such interactions can lead to frequent faults, posing significant risks to both the power grid and the environment. CCs, with their insulating layer, effectively eliminate these risks by acting as a barrier, ensuring that the conductor remains protected from direct contact with trees, branches, and animals. This significantly reduces the likelihood of faults caused by vegetation interference and importantly protects wildlife from electrocution [4].

CCs have proven to be especially beneficial in regions where traditional bare conductors are vulnerable to damage, including rural areas with dense forests and regions with high wildlife activity. In these environments, the risk of external interference with power lines is much higher, making it essential to implement reliable solutions to protect the transmission infrastructure. CCs have emerged as a robust solution in these areas, effectively addressing the challenges posed by environmental risks and wildlife threats. The insulating layer ensures that even in the most challenging conditions, the transmission system continues to operate reliably.

A unique feature of CCs is their ability to handle high surface voltage approximately 95% of the conductor's voltage, as attributed to the capacitive divider effect as shown in figure 1.3, where C_1 represents the capacitance between the conductor and the insulating layer, and C_2 corresponds to the capacitance due to the surrounding air [5]. The insulating layer, combined with air acting as a dielectric medium, ensures safety even at such high voltages, with surface currents remaining extremely low (μ A). This design not only safeguards wildlife from electrocution but also reduces maintenance needs by eliminating direct interactions with vegetation, significantly cutting operational costs.

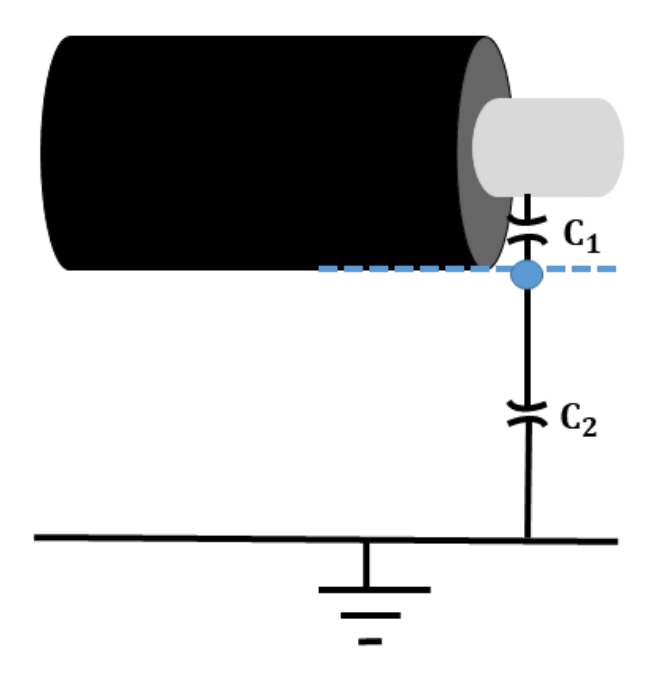


Figure 1.3 Voltage distribution of covered conductor [5]

Furthermore, the insulation helps keep moisture at bay, preventing water ingress that could otherwise cause short circuits or further degradation of the conductor. The insulating layer also acts as a buffer against temperature extremes, preventing the conductor from experiencing undue mechanical stress due to expansion and contraction caused by temperature fluctuations.

Reliability is another key advantage that CCs bring to the table as CCs ensure that power transmission remains stable and consistent. In regions prone to storms or heavy winds, where falling trees and branches can bring down power lines, CCs provide added resilience, allowing the transmission network to continue operating smoothly even during extreme

weather events. This increase in system reliability results in fewer power outages, enhancing the overall stability of the grid and reducing downtime for both utilities and consumers.

Maintenance is another area where CCs shine. Traditional overhead power lines require regular maintenance to ensure that tree branches and other obstacles do not come into direct contact with the conductors. This maintenance is often labor-intensive and costly, particularly in areas with dense vegetation. CCs, however, minimize the need for such upkeep by providing an insulation barrier that prevents contact with trees and branches. Utilities can therefore allocate resources more effectively, cutting maintenance costs and improving the overall cost-efficiency of the transmission system.

The widespread adoption of CCs has extended beyond low- and medium-voltage systems to high-voltage transmission lines, marking a significant evolution in the way power is transmitted. As technology continues to advance, CCs have become an integral part of modernizing electrical grids, offering a robust solution to challenges posed by environmental exposure, wildlife interference, and other external risks. Their use has transformed power transmission, providing enhanced safety, reduced maintenance, and improved reliability.

CCs also improve operational efficiency by reducing corona discharge and associated power losses. Corona discharge occurs when high voltage is applied to a conductor in the air, leading to energy losses and insulation degradation. The insulation layer in CC minimizes these discharges, improving transmission efficiency. Additionally, CC enables higher current-carrying capacity and facilitate upgrading existing OBC lines to higher voltage levels without requiring substantial infrastructure modifications [5]. Reduced maintenance needs further contribute to the operational efficiency of CC systems.

Looking ahead, the role of CCs in the future of power transmission is poised to grow even more crucial. As global demand for reliable and efficient electricity transmission increases, CCs will continue to play a pivotal role in ensuring that power reaches consumers safely and without disruption. With their proven advantages, CCs offer a sustainable and resilient solution for the ongoing challenges of power transmission, laying the foundation for a more reliable and efficient energy future.

1.2.1 Conductor Sleeves

Conductor Sleeves (CS) have emerged as a flexible and advanced alternative to Covered Conductors (CCs) in medium-voltage power transmission systems. Designed with insulating layers typically made of silicone rubber, CS offers comparable protection against environmental factors, vegetation contact, and wildlife interference ensuring operational safety and system reliability. Unlike CCs, however, CS feature a more adaptable and flexible construction, making them particularly suitable for installations in challenging terrains and for applications that require frequent maintenance or sectional replacements. This flexibility not only simplifies installation but also reduces operational costs, especially in networks prone to frequent upgrades or environmental stress.

The growing adoption of CS reflects the ongoing evolution of transmission technologies aimed at enhancing safety, efficiency, and adaptability. By addressing some of the inherent limitations of traditional bare conductors while complementing the functionality of CCs, CS contribute significantly to the resilience and sustainability of modern power transmission infrastructure. Subsequent chapters will delve into their construction details, challenges such as electro-thermal stresses, and a comparative performance analysis between CS and CCs highlighting their respective roles in strengthening medium-voltage networks.

1.3 Conclusions

This chapter establishes the critical role of overhead transmission lines in modern power systems, highlighting their advantages, such as cost-effectiveness and ease of maintenance, alongside challenges like faults caused by weather, vegetation, wildlife, and corrosion. It introduces covered conductors (CCs) and conductor sleeves (CS) as innovative solutions that enhance safety, reduce maintenance, and mitigate environmental and wildlife-related risks compared to traditional bare conductors. By addressing these challenges, CCs and CS improve the reliability and efficiency of medium-voltage transmission systems. The chapter sets the foundation for the thesis by emphasizing the need to investigate CS, particularly their electro-thermal performance, to optimize their design and ensure robust performance under operational stresses, paving the way for subsequent chapters to explore these aspects in detail.

Chapter 2 Literature Survey

The role of CCs in modern power transmission systems has gained considerable attention in recent years. These conductors, which are typically used to improve the safety, reliability, and performance of electrical grids, face a variety of challenges that impact their operational efficiency. While CCs offer numerous advantages, including protection against environmental factors, they also present unique challenges related to electrical tracking, partial discharge (PD), and fault conditions. This chapter explores these challenges in detail, along with the advancements in research and technology aimed at improving the performance of insulated conductors.

2.1 Electrical Tracking and thermal runaway in Covered Conductors

Electrical tracking is a gradual deterioration process that occurs on the surface of insulation materials, leading to the formation of conductive paths. These paths enable the flow of current through the insulation layer, causing localized heating, chemical reactions, and ultimately resulting in insulation failure or breakdown. The primary causes of electrical tracking are high-voltage stress combined with surface contamination, such as dust, moisture, and pollutants like salt and industrial chemicals.

The process begins with the accumulation of contaminants on the insulation surface. These contaminants compromise the insulating properties of the material when high voltage is applied, reducing its dielectric strength. This results in the formation of localized electric fields that are intense enough to ionize the surface. As ionization occurs, conductive paths develop and grow progressively due to repeated electrical discharges and the associated localized heating and chemical reactions. Over time, these conductive paths deepen and expand, causing irreversible damage to the insulation and forming permanent channels.

Electrical tracking is more pronounced in environments with high humidity, salty air, or industrial pollutants. Coastal areas, where saltwater vapours are prevalent, and industrial zones, where airborne contaminants like oils, sulphur, and chemical dust are common, are particularly vulnerable to tracking phenomena. Research has shown that the presence of contaminants significantly lowers the dielectric strength of the insulation material, increasing the likelihood of tracking initiation [6]. Polymeric insulation materials, such as ethylene

propylene rubber (EPR) and cross-linked polyethylene (XLPE), are widely used in CCs due to their excellent electrical properties and ease of processing [2]. EPR demonstrates superior performance in environments prone to electrical tracking because of its enhanced moisture resistance and thermal stability, whereas XLPE, despite its good dielectric properties, is more susceptible to tracking in high-humidity conditions, which can degrade its long-term reliability. Electrical tracking, a key aging mechanism, involves the formation of partially conductive paths on the insulation surface due to electrical discharges, often triggered by high surface electric fields, leakage currents, and surface contaminations.

Several studies have explored the effects of environmental factors on tracking resistance, with a particular focus on the influence of humidity and airborne contaminants [7]. These studies reveal that high humidity levels promote the formation of conductive paths by enhancing the ionic conductivity of the surface. Salt-laden air, typical of coastal regions, further accelerates the process, as salts provide a direct path for electrical conduction under high-voltage conditions. Understanding the causes and mechanisms of electrical tracking is critical for developing effective strategies to prevent or mitigate its impact on insulation systems.

Studies on evaluating electrical tracking resistance primarily focus on assessing material properties [8-11], with relatively few investigations delving into the electrical tracking phenomenon itself [12]. R. Fernandes da Silva at.al [6] proposed a process to explain how electrical tracking rupture occurs under humid conditions, which is depicted in figure 2.1. The process (a to f) begins with the humidification and contamination of the material surface, forming a conductive layer with low surface resistivity. When moisture and contaminants settle on the surface of an insulating material, a small surface current starts to flow. These current produces heat, which begins to dry out the moisture. As the moisture evaporates, it leaves behind dry bands—areas where current can no longer flow easily. These dry bands cause the electric field to spike in those spots, leading to tiny electrical sparks, called surface discharges.

These discharges heat the material even more, slowly damaging the surface and forming black, carbon-like marks. These marks are slightly conductive and let more current through, which produces even more heat. This creates a vicious cycle—more heat causes more

damage, and more damage allows more current, which leads to even more heat. As the temperature keeps rising, the insulation starts to lose its ability to resist electricity. It begins to behave less like an insulator and more like a conductor. This is known as thermal runaway, a point where the material can't cool down fast enough, and the heat keeps building up out of control. Eventually, the insulation is so damaged that electricity can pass right through it without resistance. At this point, the material has completely broken down, and it can no longer protect the system. This can lead to dangerous failures like short circuits or fires, especially in high-voltage systems.

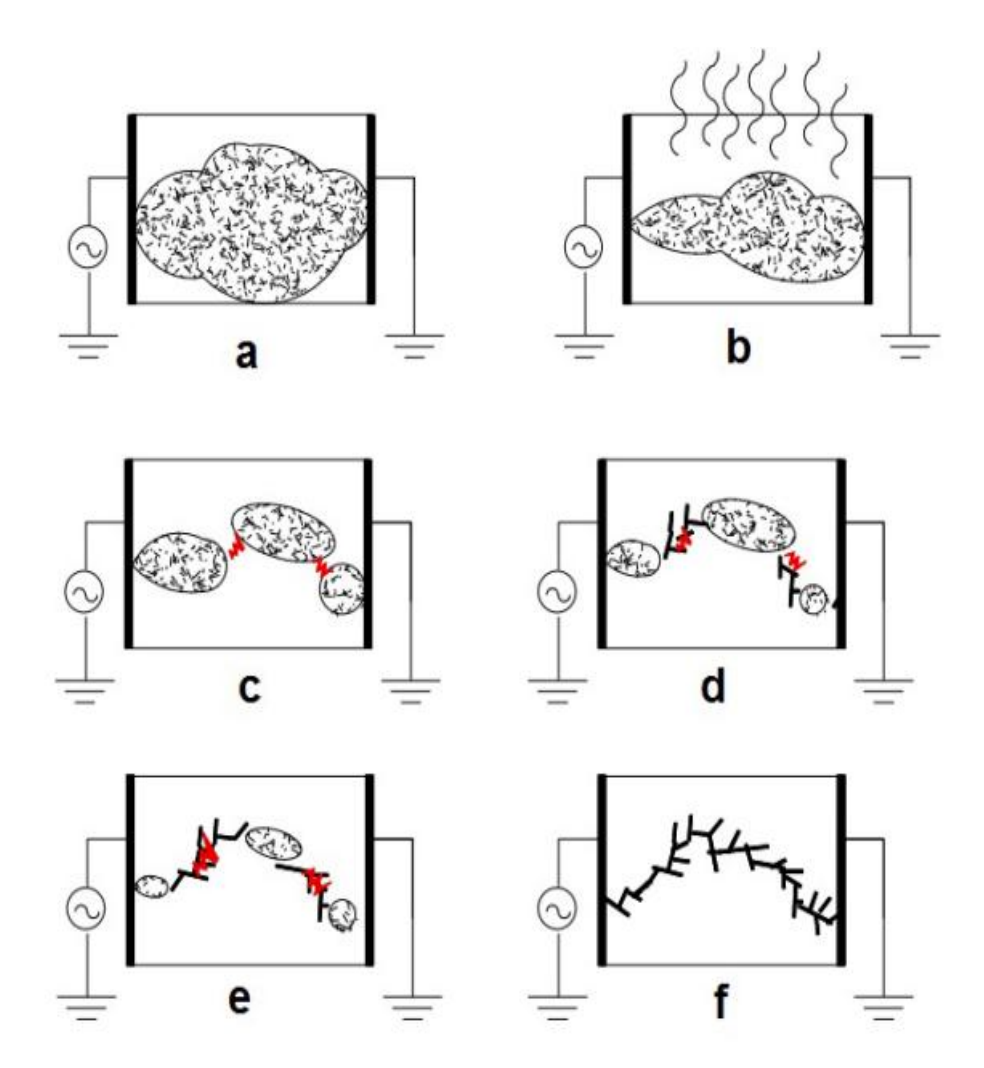


Figure 2.1 Process of electrical tracking rupture in humid environments [6]

Further, in [13] the tests were conducted on alternative solutions for spacer cable systems using materials like semiconducting tubes and tapes applied to CCs and spacers.

These tests, as shown in figure 2.2, revealed tracking and erosion issues, especially in 15 kV systems, whereas standard configurations performed better under multi-stress conditions.

Furthermore, 35 kV systems exhibited greater resistance to tracking and erosion compared to 15 kV systems, as demonstrated in [13]. This is primarily due to the increased leakage distance in 35 kV spacers, which reduces surface electric field intensity and mitigates partial discharges under polluted conditions. Thicker insulation in 35 kV systems also enhances resistance to erosion by providing more material to withstand discharge-induced degradation.



Figure 2.2 Semiconducting tube placed on CC to investigate tracking [13]

Several methods developed to evaluate the tracking and erosion resistance of aiming to compare and categorize the voltage levels observed in practical applications materials [14-17]. These techniques utilize various parameters to assess the correlation between a material's ability to resist electrical tracking. Among the commonly employed methods are the fog-anddust test [14] and the threshing wheel test [15], which rely heavily on visual inspection for evaluation. In these methods, the author's suggestions plays a critical role in determining whether visible tracks have formed on the material's surface. The fog-and-dust method involves exposing the material to a controlled environment of moisture and particulate matter, while the threshing wheel test subjects the material to dynamic stress conditions. Both methods classify materials based on the presence or absence of discernible tracking marks, making them effective tools for assessing material performance under different environmental and electrical conditions. Thus, preventing electrical tracking is not only crucial for avoiding surface degradation but also essential for halting the onset of electrothermal runaway and complete insulation failure. Effective material selection, insulation design, and testing protocols are critical in enhancing the long-term safety and performance of high-voltage insulation systems.

2.2 Mitigation Strategies for Electrical Tracking

Several strategies have been developed to mitigate electrical tracking in CCs. One approach involves enhancing the hydrophobic properties of the insulation material through surface treatments, such as the application of Nano coatings, silicone-based materials, and hydrophobic polymers. These treatments reduce the adhesion of contaminants to the surface, thereby decreasing the likelihood of tracking initiation. For instance, super hydrophobic coatings have been extensively reviewed for their effectiveness in outdoor high-voltage insulation applications [18].

Another strategy focuses on improving the material's resistance to chemical degradation. Researchers are developing new polymeric compounds that offer better resistance to environmental factors like UV radiation, ozone, and temperature fluctuations. By enhancing the chemical stability of the insulation material, it becomes more resilient to tracking over time. Studies have investigated the impact of accelerated ultraviolet weathering on polymeric materials, highlighting the importance of material selection in maintaining insulation performance [19]. Additionally, the degradation and stability of polymeric high-voltage insulators examined to understand their performance under various environmental conditions, emphasizing the need for materials with improved resistance to chemical degradation [20].

2.3 Partial Discharge in Covered Conductors

Partial discharge (PD) refers to localized electrical discharges occurring within voids, cracks, or defects in insulation materials, leading to gradual degradation and eventual failure [21-22]. In covered conductors (CCs), PD often goes undetected, resulting in latent damage that accelerates insulation deterioration and increases the likelihood of catastrophic failures, such as power outages [23]. Contributing factors include manufacturing defects, improper installation, aging of insulation materials, and adverse environmental conditions [21-23]. Time-Domain Reflectometry (TDR) is a widely used technique for locating PD, relying on reflections caused by insulation defects, with studies demonstrating its effectiveness in online PD localization for CC systems [24]. Ultra-High-Frequency (UHF) measurements, on the other hand, detect electromagnetic signals generated by PD, enabling real-time monitoring and accurate analysis even in high-noise environments [25]. Together, these methods provide a comprehensive framework for assessing insulation integrity. However, the analysis of PD is beyond the scope of this thesis.

2.4 Fault Conditions in Covered Conductors

Covered conductors are susceptible to several types of faults, including short circuits and ground faults. Short circuits occur when the insulation fails, allowing the conductor to come into direct contact with another phase or the ground.

Therefore, thermal overloads conditions may arise due to excessive current can degrade insulation materials over time. These faults can lead to significant energy losses, equipment damage, and safety hazards and power outages, thus necessitating robust design and monitoring systems to mitigate their impact.

2.4.1 Causes of Faults in Covered Conductors

Faults in covered conductors (CCs) are caused by several factors, including insulation breakdown, mechanical stresses, and external damage. Insulation degradation is often attributed to prolonged exposure to environmental elements such as UV radiation, extreme temperature variations, and chemical contaminants, which reduce the dielectric strength of the material over time. Mechanical stresses, including conductor sag, abrasion, and vibrations due to wind or load changes, can further exacerbate insulation wear and tear, leading to failure.



Figure 2.3 Example of a high-impedance fault occurs when tree branches come into contact with overhead CCs [26].

External factors affecting the CCs performance such as wildlife interference, physical impacts from storms, falling branches, or accidental collisions as shown in figure 2.3,

significantly contribute to fault conditions. These faults compromise the safety and reliability of electrical systems, causing power outages and increasing maintenance demands. Therefore, robust designs, enhanced materials, and regular monitoring are essential to mitigate these challenges [26].

2.4.2 Protective Measures and Fault-Tolerant Designs

To mitigate fault conditions in CCs researchers are developing advanced protective coatings and insulation designs to improve material robustness. Fault-tolerant designs, such as segmented insulation systems, are being explored to localize fault impacts and streamline maintenance procedures [27]. Segmented insulation systems feature multiple insulation layers separated into distinct sections, enabling easier identification and isolation of faulted areas. This modular design allows replacement of only the damaged segments, reducing downtime and maintenance costs.

The performance of these insulation systems is closely tied to the material's electrical properties, particularly complex permittivity (ϵ^*), which governs the response of dielectrics to an applied electric field. Complex permittivity is expressed as

$$\varepsilon^* = \varepsilon' - j\varepsilon'' \tag{2.1}$$

Where: ε' is the real part of the permittivity represents the material's ability to store electrical energy referred as the dielectric constant, and ε'' represent imaginary part, quantifies the energy dissipation within the material, also known as dielectric loss. The ε'' component of complex permittivity holds good co-relation with the AC conductivity as depicted in equation (2.2), and it plays a critical role in thermal instability, as increased energy dissipation can lead to excessive heat generation, ultimately causing the material to undergo complete breakdown.

$$\sigma_{AC} = \omega \varepsilon_0 \varepsilon'' \tag{2.2}$$

where ω is the angular frequency and ε_o is the permittivity of free space. High ε'' values indicate increased energy dissipation, which can exacerbate thermal instability and lead to insulation breakdown under fault conditions. By selecting materials with optimized ε' and minimized ε'' for insulation systems, designers can enhance fault tolerance and reduce the risk of catastrophic failures.

In addition to advanced insulation designs, researchers are developing diagnostic tools to improve fault detection and localization. These tools employ fault-location algorithms that leverage data from real-time monitoring systems to precisely identify fault locations in CCs. Incorporating measurements of complex permittivity and AC conductivity into these diagnostic systems can further enhance their accuracy. For instance, variations in ϵ " or σ_{AC} , detected through spectroscopy or other techniques, can signal early degradation or fault initiation in insulation materials. By integrating such material property data with real-time monitoring, these systems enable faster and more efficient repair processes, minimizing disruptions and ensuring the reliability of power transmission networks [28].

2.4.3 Limitations of Covered Conductors

Despite the numerous benefits of covered conductors (CCs), certain drawbacks limit their widespread adoption. A significant issue is the stiffness of the polymer insulation, which reduces the conductor's flexibility. This lack of flexibility makes CCs less ideal for installations in locations with sharp curves, irregular terrains, or constrained spaces, such as urban or mountainous regions. Another notable drawback is the increased weight of covered conductors compared to bare conductors. The added weight complicates the installation process, often requiring specialized tools and techniques. Furthermore, damage to the insulation layer caused by faults or other factors frequently necessitates replacing the entire CCs lines. This approach can be expensive and time-intensive, particularly in remote or hard-to-reach locations.

2.5 Conductor Sleeves in Medium Voltage System

Conductor sleeves (CS) have emerged as a pivotal innovation in medium voltage (MV) overhead transmission system, offering enhanced safety, flexibility, and operational efficiency compared to traditional overhead bare conductors (OBC) and covered conductors (CCs). Unlike CCs, which are characterized by a rigid polymeric insulation layer, CS utilize flexible insulating materials, typically silicone rubber, enabling easier installation in challenging terrains and facilitating sectional replacements. This section reviews the applications of CS in MV systems, synthesizes prior research on their electro-thermal performance, and identifies critical research gaps that underscore the novelty of this thesis.

2.5.1 Applications of Conductor Sleeves in Medium Voltage Systems

Conductor sleeves are primarily employed in MV transmission networks (typically 11 kV to 35 kV) to mitigate risks associated with environmental exposure, vegetation contact, and wildlife interference. Their flexible design allows for retrofitting onto existing OBCs, enabling cost-effective upgrades to higher voltage levels without extensive infrastructure modifications. CS are particularly advantageous in rural or forested areas, where tree branches or wildlife can cause high-impedance faults, as depicted in figure 2.4. By providing an insulating barrier, CS reduce the likelihood of faults, protect wildlife from electrocution, and minimize fire risks, thereby enhancing system reliability. Additionally, CS offer practical benefits in maintenance and installation. Their flexibility simplifies handling in regions with sharp curves or irregular terrains, addressing the stiffness limitations of CCs. Unlike CCs, which often require replacement of entire lines when damaged, CS can be replaced sectionally, reducing downtime and operational costs. These attributes make CS an attractive solution for modernizing MV grids, particularly in areas prone to environmental stresses.

2.6 Motivation

The increasing demand for safer, more efficient, and reliable power transmission systems has driven the development of innovative solutions to address the limitations of traditional overhead bare conductors (OBC). Among these advancements, covered conductors (CC) and conductor sleeves (CS) have emerged as transformative technologies, offering improved safety, operational efficiency, and environmental protection. However, CCs present challenges such as rigidity, which complicates installation in varied transmission environments, and their replacement often involves significant downtime and expense. In contrast, conductor sleeves (CS) provide greater flexibility, making them adaptable to diverse installation scenarios, and they can be more easily replaced when required, thereby reducing maintenance complexity and costs. Despite these advantages, CS face their own set of challenges, including degradation and tracking issues, which limit their broader adoption.

This study is motivated by the need to overcome these limitations and optimize the design and performance of CS for medium-voltage systems. A particular focus is given to understanding and mitigating critical phenomena such as electrical tracking and electrothermal runaway in CS. By addressing these challenges, this research aims to enhance the

long-term reliability and adaptability of power transmission infrastructure, supporting the transition to safer, more resilient, and sustainable energy systems.

2.7 Problem Statement

The adoption of conductor sleeves (CS) in modern power systems is growing rapidly, driven by their numerous advantages over traditional overhead bare conductors (OBC) and covered conductors (CC). The CS offer enhanced durability, flexibility, and system stability while significantly reducing power losses, operational expenses, and environmental risks such as forest fires. Additionally, CS enables cost-effective upgrades of OBC lines to higher voltage levels without requiring substantial infrastructure modifications.

The silicone rubber (Si-R) made conductor sleeves as shown in figure 2.4 is highly flexible, making them suitable for installation in challenging terrains, including hilly areas or locations requiring sharp turns. This flexibility, combined with ease of replacement in the event of faults, ensures a cost-effective and practical solution for modern power utilities. CS efficiently replaced with minimal expense and effort, further increasing their appeal as a superior alternative to traditional designs.



Figure 2.4 Medium voltage AC conductor sleeves: (a) Cross sectional view of CS (b)

Implementation of CS on transmission Systems [29]

Given the availability of various CS designs, it is crucial to determine the optimal configuration based on performance requirements; however, the long-term reliability and safety of CS are constrained by electro-thermal challenges, including tracking and thermal

runaway phenomena. These issues necessitate a deeper understanding of the mechanisms governing the behavior of CS. The challenges in the areas with complex environmental conditions, such as proximity to vegetation or wildlife, can induce additional stress through physical contact with the sleeves. A critical factor in the performance of CS design of their overlapping insulation layers, which serve as protective barriers against environmental and electrical stresses.

As the unique dynamics of CS, particularly in their overlapping regions (90° and 180°), remain under-investigated. This study aims to fill these gaps by investigating the tracking and electro-thermal runaway phenomena in SCR-based CS designed for MV systems. In this research, a novel measurement method developed to evaluate the AC conductivity on the surface and at the interface of CS. These measurements are used to find other dielectric parameters essential for assessing insulation performance. The obtained data incorporated into finite element method (FEM) software for comprehensive electro-thermal analysis. Correlating the results with experimental findings, the most efficient and adaptive CS design identified upon analysis, and, ensuring improved performance, reliability for power transmission systems.

2.8 Applicability of Covered Conductors and Conductor Sleeves Across Voltage Levels

Covered conductors (CC) and conductor sleeves (CS) have emerged as critical solutions for enhancing the safety, reliability, and environmental resilience of overhead power transmission systems. While this thesis primarily focuses on medium-voltage (MV, 11–35 kV) systems, where CC and CS are widely adopted, their applicability across low-voltage (LV, <1 kV) and high-voltage (HV, >35 kV) systems warrants detailed consideration. This subsection discusses the suitability, practical limitations, and design considerations of CC and CS across these voltage levels, with a particular emphasis on the challenges posed by increased weight at higher voltages.

I. Low-Voltage Systems (<1 kV)

In LV systems, typically used for residential and small commercial distribution, the adoption of CC and CS is limited due to lower fault risks and cost considerations. Bare conductors are generally sufficient in LV networks, as the reduced voltage levels minimize the risk of arcing, flashovers, or vegetation-induced faults. However, in specific scenarios—such as urban areas with dense vegetation, coastal regions with high humidity, or locations with significant

wildlife activity—CC may be employed to enhance safety and reduce maintenance. For instance, CC insulated with cross-linked polyethylene (XLPE) can protect against environmental degradation, as noted in Section 1.2. CS, designed for flexibility and ease of replacement, are rarely used in LV systems, as their benefits are more pronounced in MV applications where tracking and electro-thermal runaway are significant concerns. The added cost and weight of CC or CS in LV systems are typically not justified unless specific environmental or safety requirements necessitate their use.

II. Medium-Voltage Systems (1–35 kV)

MV systems, the primary focus of this thesis, represent the most common application for CC and CS due to their ability to mitigate vegetation-induced faults, wildlife electrocution, and environmental stresses. These systems are prevalent in rural and forested areas, where high-impedance faults caused by tree branches or animals are frequent. CC, typically insulated with XLPE or ethylene propylene rubber (EPR), provide robust protection against such faults, while CS, made of silicone rubber (Si-R) with 90° or 180° overlapping configurations, offer flexibility and ease of installation. The manageable weight of CC and CS in MV systems allows for installation on standard support structures without significant modifications, even in challenging terrains such as hilly or forested areas.

III. High-Voltage Systems (>35 kV)

CC and CS have been implemented in select HV applications, including voltages up to 220 kV, particularly in regions where environmental challenges (e.g., dense vegetation, coastal pollution) necessitate enhanced insulation [4, 13]. However, their use in HV systems is less common due to significant practical limitations. The higher electric field stresses in HV systems require substantially thicker insulation to prevent partial discharges, corona effects, and dielectric breakdown. For example, while MV CS in this study use 7–10 mm of insulation thickness, HV applications require to increase insulation thickness, leading to increased weight, sag, and mechanical stress on support structures. This added weight complicates installation, particularly for long spans, and increases costs due to the need for reinforced towers or closer pole spacing. Additionally, corona discharge, a significant concern at HV levels, can degrade insulation and increase power losses, necessitating specialized materials and designs (e.g., high-performance polymers or nano-enhanced composites) that further escalate costs [18]. CS face similar challenges in HV systems, as

their overlapping design (90° or 180°) may not provide sufficient dielectric strength without significant modifications, such as multi-layer insulation or increased thickness, which exacerbate weight-related issues.

The applicability of CC and CS varies significantly across voltage levels due to differences in dielectric requirements, mechanical constraints, and cost considerations. While MV systems benefit greatly from the safety and reliability offered by CC and CS, their use in LV systems is limited by cost, and in HV systems by weight, sag, and corona-related challenges. Future advancements in lightweight materials, optimized geometries, and multi-layer insulation designs, as discussed in Section 6.2, could enhance their feasibility for HV applications, supporting the transition to safer and more resilient power transmission systems.

2.9 Chapter-Wise Contributions to the Thesis

This thesis systematically investigates the interfacial electro-thermal dynamics of conductor sleeves (CS) in medium-voltage AC systems, with each chapter contributing distinct insights and advancements to the field. Below is a summary of the contributions of each chapter.

Chapter 1: Introduction

This chapter establishes the foundation of the research by highlighting the role of overhead transmission lines and the evolution from bare conductors to covered conductors (CCs) and conductor sleeves (CS). It identifies key challenges, such as faults due to environmental factors, wildlife, and corrosion, and underscores the need for reliable insulation solutions. The contribution lies in providing a comprehensive context for the study, emphasizing the advantages of CS, such as flexibility and cost-effectiveness, over CCs, and setting the stage for investigating electro-thermal challenges in medium-voltage systems.

Chapter 2: Literature Survey

This chapter provides a comprehensive review of existing research on electrical tracking, partial discharge (PD), and fault conditions in covered conductors (CCs), identifying gaps in understanding CS performance. It introduces CS as a novel solution and defines the problem statement, focusing on optimizing CS designs for tracking resistance and electro-thermal stability. The contribution lies in establishing the research gaps, particularly the lack of studies on interfacial dynamics in CS and motivating the investigation of 90° and 180° overlapping configurations to enhance reliability.

Chapter 3: AC Conductivity Measurement

This chapter develops novel experimental setups to measure AC conductivity in the volumetric, surface, and interfacial regions of CS under varying temperatures and electric fields. It reveals that interfacial conductivity is significantly higher, identifying the interface as the primary site for tracking initiation. The contribution includes providing critical conductivity parameters for FEM simulations, validated through curve-fitting, and laying the groundwork for modelling electro-thermal behaviour in CS.

Chapter 4: FEM Modelling Analysis and Validation of Conductor Sleeves Performance

This chapter presents a detailed FEM-based analysis of CS with 90° and 180° overlapping configurations, validated through experimental measurements of interface tracking inception voltage (ITIV). It demonstrates that the 180° CS outperforms the 90° CS and CCs due to reduced electric field intensity, with findings validated by experimental results. The contribution lies in providing a validated simulation framework for electro-thermal analysis, recommending the 180° CS for medium-voltage applications, and suggesting insulation thickness adjustments for the 90° CS to enhance reliability.

Chapter 5: Impact of Load Current on the Performance of Conductor Sleeves

This chapter investigates the effects of load current on CS performance, focusing on thermal and electrical stresses. It shows that load current reduces ITIV due to thermal aging, but applying insulation tape at the interfacial region increases ITIV by 5.0% to 7.9%. FEM simulations under loaded conditions further highlight the role of thermal stress in accelerating runaway. The contribution includes practical insights into CS performance under operational conditions, a cost-effective solution (insulation tape) to enhance dielectric strength, and recommendations for considering load effects in CS design.

Chapter 6: Conclusions and Future Work

This chapter synthesizes the findings, concluding that the 180° overlapped CS is the most reliable for medium-voltage systems due to its superior tracking resistance and adaptability. It identifies the interfacial region as the most vulnerable to run-away and proposes insulation enhancements. The contribution lies in consolidating the thesis's findings into actionable recommendations for industry applications and outlining future research directions, such as

long-term aging tests and advanced insulation methods (e.g., nanocoating's), to further improve CS performance.

2.10 Conclusions

The literature survey provides a comprehensive review of electrical tracking, partial discharge (PD), and fault conditions in CCs. It identifies electrical tracking as a primary cause of insulation degradation, driven by high-voltage stress and environmental contaminants, with polymeric materials like EPR and XLPE showing varying resistance. Mitigation strategies, such as superhydrophobic coatings and advanced material designs, are discussed, alongside fault-tolerant designs like segmented insulation systems. The chapter underscores the limitations of CCs, such as stiffness and increased weight, motivating the exploration of CS as a flexible alternative. The problem statement focuses on optimizing CS designs by investigating tracking and electro-thermal runaway in 90° and 180° overlapping configurations to enhance reliability and adaptability.

CS have a unique design, particularly in their overlapping regions (90° or 180°). These entire CS design bifurcated into three parts: volumetric, interfacial, and surface, as shown in figure 3.1. To ensure the effective design and performance of CS, it is important to study these regions by examining key factors like dielectric properties, tracking behaviour, and electrothermal runaway phenomena.

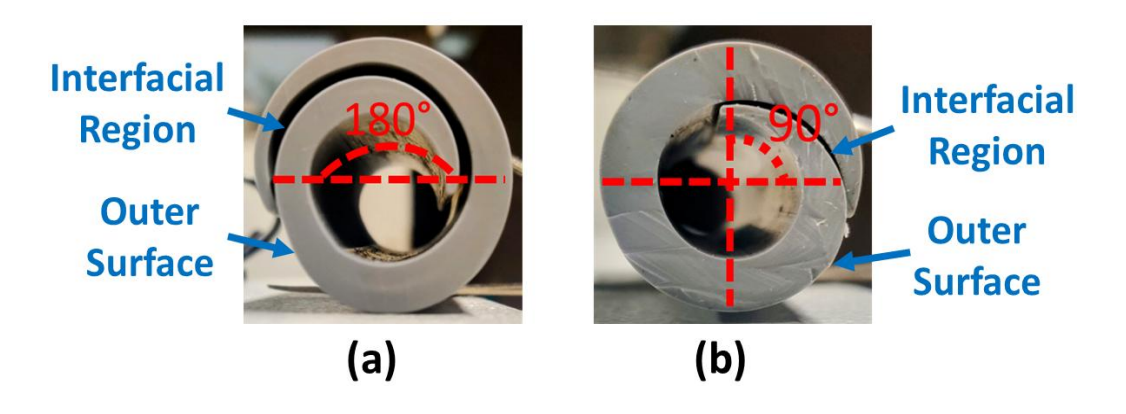


Figure 3.1 Silicon rubber-based CS: (a) 180° overlapping angle (b) 90° overlapping angle configuration.

A critical part of this evaluation involves measuring the AC conductivity of the surface, interface, and volumetric regions. These measurements provide valuable insights into how the CS will perform under different conditions, such as varying voltages, electric field and temperatures.

This chapter explains the methods and steps used to carry out these measurements in detail, providing a clear understanding of the procedures necessary to assess the performance of CS in power transmission systems.

3.1 AC volumetric Current Measurement

To determine the volumetric AC conductivity of CS, dielectric spectroscopy was conducted using a structured procedure. Samples were prepared by cutting the SCR sheets from freshly produced CS provided by a local manufacturer. After visual inspection, the sheets were cleaned with ethanol to eliminate any surface contaminants. They were then precisely cut into 13 mm diameter circular discs with a uniform thickness of 0.7 mm (±0.01 mm), slightly

larger than the 10 mm diameter of the brass electrodes (test cell electrode) to reduce edge effects. The measurement setup featured a parallel-plate test cell with polished brass contacts, ensuring even electric field distribution. Each sample was placed between the electrodes and held firmly using a spring-loaded clamp. A guard ring was used to suppress surface leakage currents during testing. To ensure accurate measurement and eliminate any moisture, the samples were kept in a temperature-controlled oven at 50°C for 48 hours before testing [30].

Dielectric spectroscopy measurements were carried out using the Novo-control system. Tests were conducted at three applied voltages 70 V, 700 V, and 1050 V corresponding to electric field strengths of 0.1 kV/mm, 1.0 kV/mm, and 1.5 kV/mm for the 0.7 mm thick samples. At each field level, measurements were taken at three temperatures: 293.15 K, 323.15 K, and 343.15 K, resulting in nine unique test conditions.

This setup allowed for precise observation of the material's behavior under varying thermal and electrical stresses. The results obtained from the dielectric spectroscopy provide complete information about dielectric constant (ϵ'), dielectric loss (ϵ''), complex permittivity, loss tangent. These measurements help in understanding AC conductivity, polarization mechanisms, charge transport, and material performance under electric fields, especially in insulation applications like Conductor Sleeves (CS).

The AC volumetric conductivity of the CS material holds good correlation with both temperature and the applied electric field. To analyse the data, the volumetric conductivity using equation (2.2) was fitted to a mathematical model represented by following equation [31-32].

$$\sigma(T, E) = Ae^{\alpha E - \frac{\beta}{T}} \tag{3.1}$$

where, σ represents ac conductivity in S/m, T and E represent temperature in K and electric field (rms) in kV/mm respectively, whereas A, α and β are the conductivity coefficient (S/m), electric field coefficient (m/V) and temperature coefficient (K) respectively.

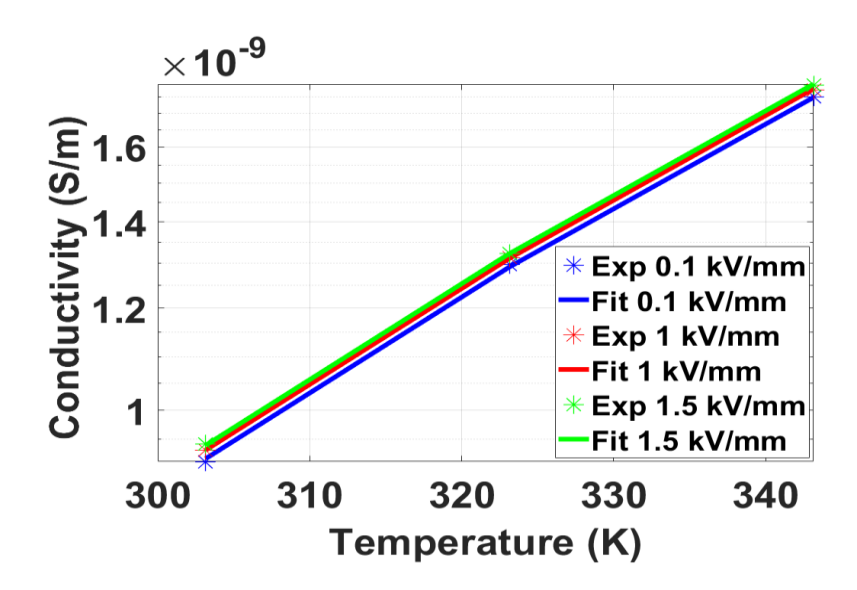


Figure 3.2 Volumetric ac conductivity of CS with respect to temperature and electric field: experimental and curve fitted.

TABLE 3.1
Estimated coefficients & goodness of fit statistics

Material	A	α	β	R ²	SSE
	(S/m)	(m/V)	(K)		
SCR	2.235×10 ⁻⁰⁷	1.70×10 ⁻⁸	1678	0.999	0.0001

These coefficients are estimated and summarized in table 3.1 using the least square curve fitting method and, the obtained plot is shown in figure 3.2, show a clear trend that both temperature and electric field increases with increased conductivity offering valuable insights into the dielectric properties and performance of the CS material.

3.2 Surface current Measurement

Measuring surface currents is essential for analyzing and understanding the tracking phenomenon, as it offers valuable information about the dielectric properties of conductor sleeve (CS) surfaces. However, despite its importance, this area remains relatively underexplored in existing research. To fill this gap, the authors introduce an innovative experimental setup designed to enable precise surface current measurements.

The proposed setup, illustrated in figure 3.3, features a configuration of three electrodes arranged uniformly, adhering to the guidelines outlined in ASTM standards [33]. In this arrangement, electrode B functions as the high-voltage (HV) electrode, while electrodes A and C act as the measuring electrodes.

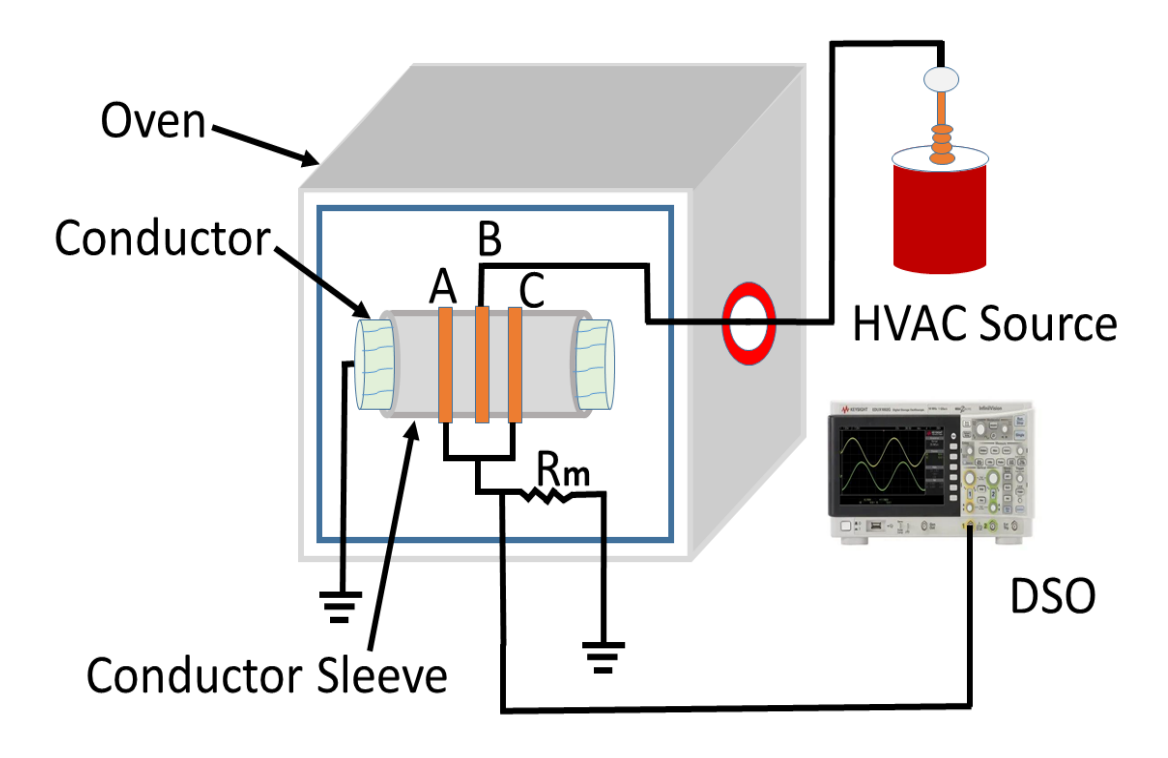


Figure 3.3 Schematic diagram for surface current measurement on CS.

To address volumetric current effects, the solid conductor, encased by the conductor sleeve (CS), is grounded, thus volumetric current mitigated. The electrodes A and C are connected at a common point, which is routed through a measuring resistor Rm (100 k Ω) and subsequently linked to a digital storage oscilloscope (DSO) for signal acquisition. This setup is designed to monitor surface current characteristics under controlled conditions. The entire assembly is housed inside an oven to ensure a stable and adjustable thermal environment, as illustrated in figure 3.4. Experimental tests were conducted with applied voltages of 1 kV, 2 kV, and 3 kV, at temperatures of 303.15 K, 323.15 K, and 343.15 K, respectively, to assess the effects of temperature and voltage on surface current behaviour.

The dielectric surface is approximated using an equivalent circuit diagram, as shown in figure 3.5(a), which provides a simplified representation of the dielectric's electrical behaviour. Figure 3.5(b) further illustrates the detailed circuit diagram of the experimental setup,

highlighting connections, components, and key parameters. The technique operates by simultaneously measuring the applied voltage, the voltage drops across Rm and the phase angle difference between these two quantities. These measurements allow for the calculation of the dielectric's equivalent impedance using equation (3.2 & 3.3) under the given experimental conditions. This impedance serves as a crucial parameter for understanding the dielectric properties of the material, enabling better characterization of its performance and potential vulnerabilities.

Dielectric equivalent impedance
$$(Z) = Z_r - jZ_i$$
 (3.2)

Where,

$$Z_r = \frac{R}{1 + \omega^2 R^2 C^2}$$
 and, $Z_i = \frac{\omega C R^2}{1 + \omega^2 R^2 C^2}$ (3.3)

Where,

 Z_r = real value of dielectric impedance and, Z_i = Imaginary value of dielectric Impedance

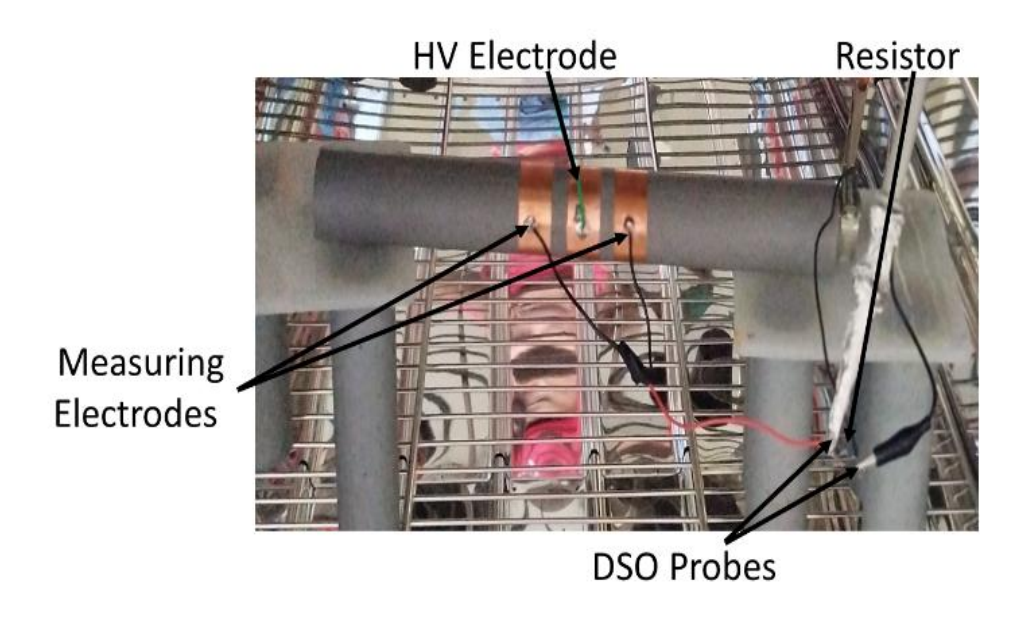


Figure 3.4 Experimental setup for surface current measurement (inside oven view)

The voltage applied on electrode B causes the current to flow on the surface of CS; measuring this current directly is a challenging task, thus, to simplify and facilitate measurement, an additional measuring resistor R_m of $100k\Omega$ as shown in figure 3.3 is introduced in series with CS. Despite the inclusion of R_m , the surface insulating impedance

remains dominant due to its high magnitude, causing the maximum voltage to drop across the surface of CS, rendering the measurement of voltage across R_m more protective and approachable.

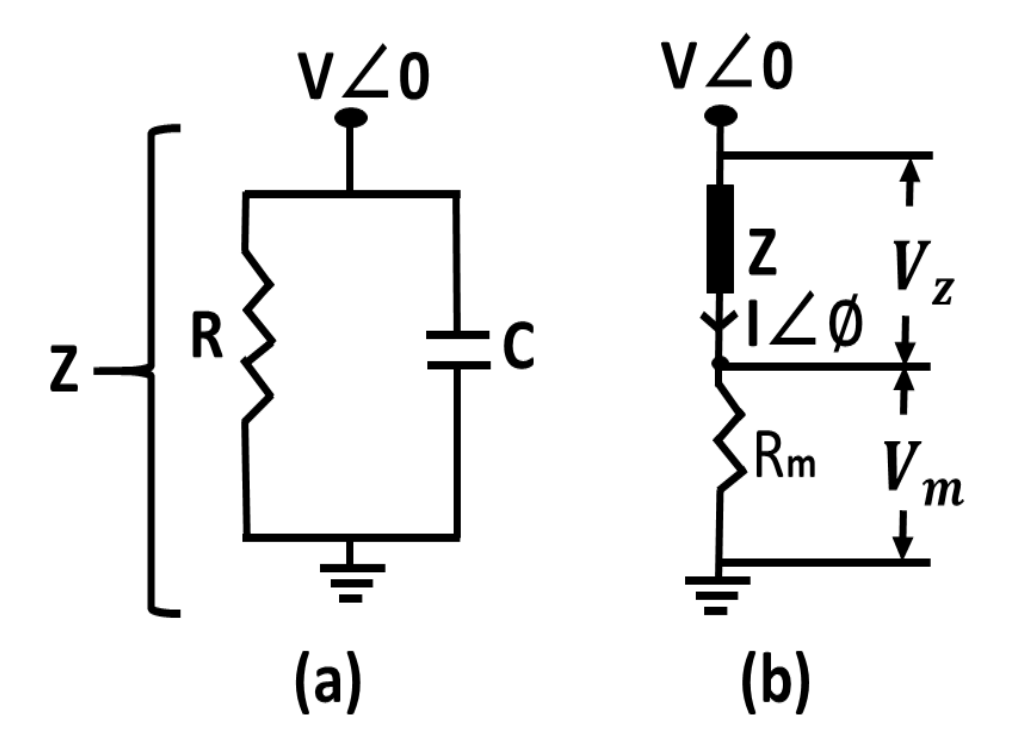


Figure 3.5. (a) Representation of equivalent circuit of dielectric (b) equivalent circuit of proposed setup.

The mathematical expressions used to calculate the surface current and AC conductivity of the conductor sleeve (CS), as depicted in figure 3.5(b), are described below

$$V \angle 0 = V_z \angle - \emptyset_z + V_m \angle \emptyset \tag{3.4}$$

Where, V_z , \emptyset_z represent the magnitude and phase angle of the surface voltage respectively.

The voltage V_m is measured on the DSO and its phase angle \emptyset is found out using equation (3.5).

$$\emptyset = \frac{\omega \Delta t}{\pi} \times 180 = tan^{-1}(\omega CR)$$
 (3.5)

Here, ω represents the angular frequency, and Δt denotes the time difference between the zero-crossing points of the applied voltage (V) and the measured voltage (V_m) as illustrated in

figure 3.6. The surface current flowing through the sleeve can then be determined using Equation (3.6).

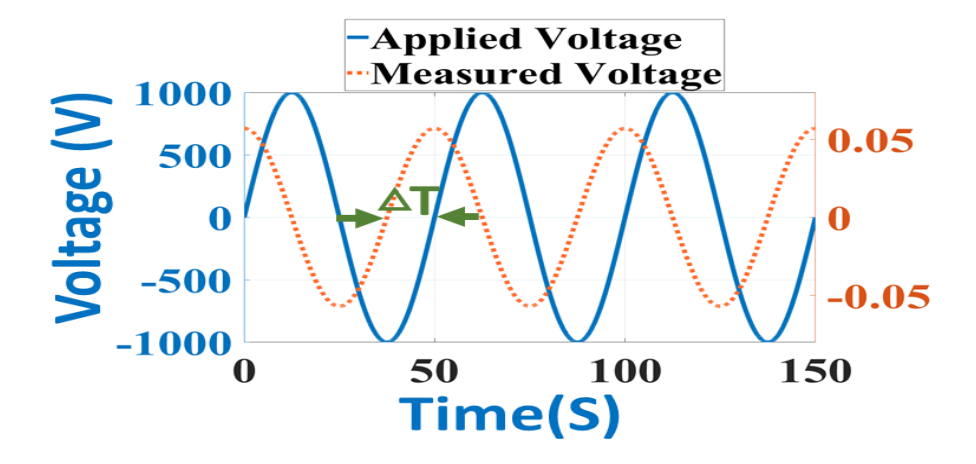


Figure 3.6 Measured voltage at 1 kV at 303.15 K.

$$I \angle \emptyset = \frac{V_m \angle \emptyset}{R_m} \tag{3.6}$$

Also,

$$Z = \frac{V_Z \angle - \emptyset_Z}{I \angle \emptyset} = Z_r - jZ_i \tag{3.7}$$

This process involves extracting the measured surface voltage and current using equation (3.4) and (3.6) respectively and subsequently utilizing these values to calculate the dielectric impedance Z, is expressed in equation (3.7).

Thus, using equation (3.3) and (3.7), the insulation surface resistance (R) and capacitance (C) are calculated. Subsequently, these values are utilised to evaluate the AC conductivity and resistivity following the standard [33], the expression to obtain the surface resistivity (ρ_s) expressed below.

$$\frac{1}{\sigma} = \rho_s = \left(\frac{P}{g}\right)R\tag{3.8}$$

Where, $P = \pi D$ is the perimeter of electrode, g is the gap between the electrodes (10 mm), and, D is the diameter of electrode. The results obtained are tabulated in table 3.2.

TABLE 3.2

Measured surface AC resistivity and conductivity for different applied voltages and temperatures

Volt	T	I	Ø	$ ho_{ m s}$	$\sigma_{\rm s}$
(V)	(°C)	(μΑ)	(degree)	(Ω)	(S)
1000	30	70	83.6	1.76×10 ¹¹	5.68×10 ⁻¹²
	50	69	82.8	1.48×10 ¹¹	6.75×10 ⁻¹²
	70	65	81	1.26×10 ¹¹	7.93×10 ⁻¹²
2000	30	74	80.1	1.05×10 ¹¹	9.52×10 ⁻¹²
	50	72.5	78.48	0.983×10 ¹¹	10.17×10 ⁻¹²
	70	68	77.4	0.88×10 ¹¹	11.36×10 ⁻¹²
3000	30	78	77.2	0.76×10 ¹¹	13.15×10 ⁻¹²
	50	74	73.8	0.68×10 ¹¹	14.70×10 ⁻¹²
	70	70	72	0.61×10 ¹¹	16.39×10 ⁻¹²

The analysis of the runaway phenomenon in conductor sleeves (CS) requires establishing a relationship between the electric field, temperature, and conductivity. This is achieved using a widely recognized semi-empirical equation (3.1), where σ represents the AC conductivity (S), T denotes temperature (K), and E is the electric field (in kV/mm). The coefficients A, α and β correspond to the conductivity coefficient (S), electric field coefficient (m/V), and temperature coefficient (K), respectively.

These coefficients obtained by applying the least-squares curve-fitting method to experimental data, the results, along with the statistical measures of fit quality, are summarized in table 3.3, and the corresponding plots are shown in figure 3.7, reveals that

temperature, conductivity and electric field phenomena are interrelated. As the temperature increases both electric field and conductivity increases like the measured volumetric conductivity in the previous section.

TABLE 3.3
Estimated surface coefficients of CS and goodness of fitting

Material	A	α	β	R^2	SSE
	(S)	(m/V)	(K)		
SCR	3.36×10 ⁻¹¹	3.94×10 ⁻⁶	645.6	0.99	0.003

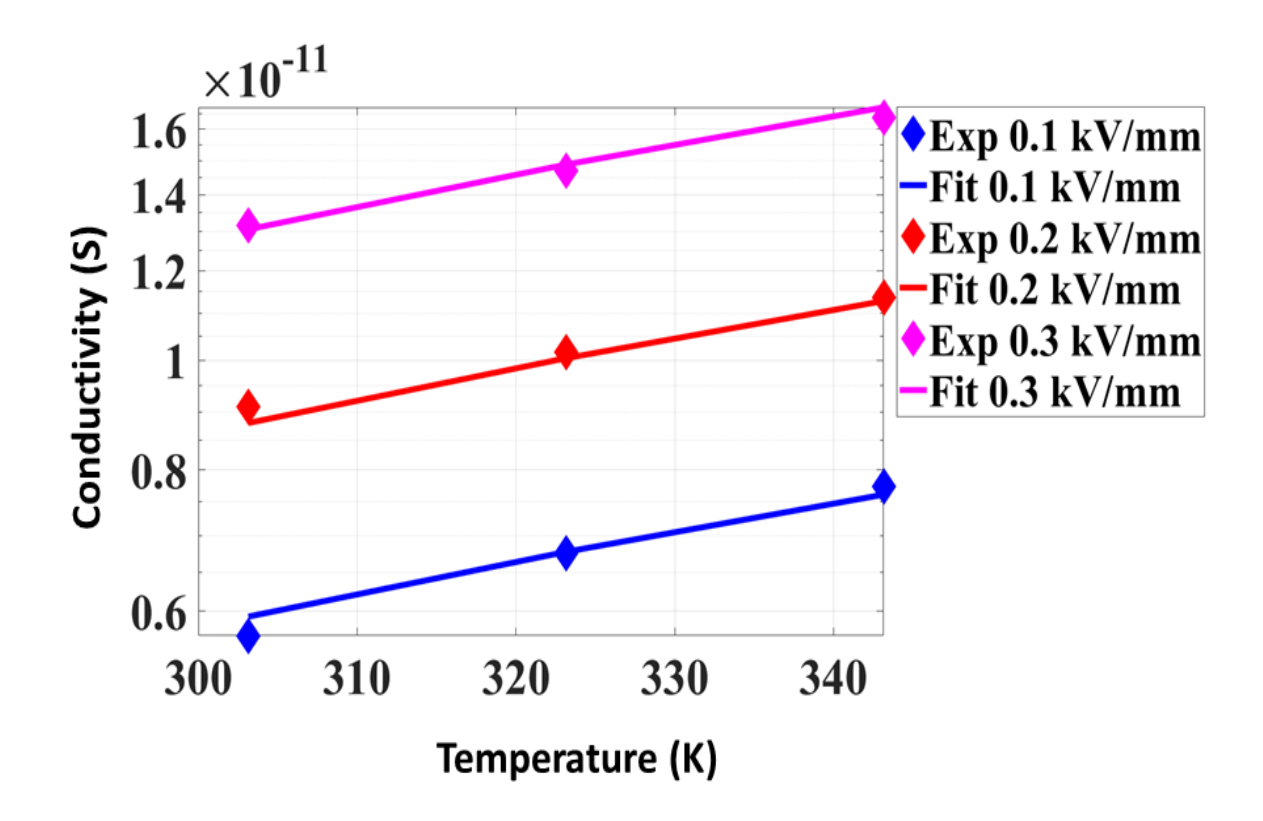


Figure 3.7 Surface conductivity of CS with respect to temperature and electric field: experimental and curve fitted.

This arrangement ensures consistency and reliability in the measurements. This experimental setup accurately measures surface current under different conditions, producing reliable and consistent results. It allows for a thorough study of the dielectric properties of Conductor Sleeves (CS) surfaces, shedding light on how electrical tracking begins and spreads. The surface conductivity data gathered from these experiments is incorporated into a Finite

Element Method (FEM) model, enabling a deeper exploration of tracking and runaway behaviors in CS. This method greatly improves the understanding of the mechanisms driving CS performance and fills an important gap in current knowledge. Moreover, it lays the groundwork for future research and development to enhance the design, performance, and reliability of conductor sleeve materials for a wide range of applications.

3.3 Interface Current Measurement

As shown in figure 3.1, the current does not only flow along the surface of the CS but also passes through the overlapping region or interface between the CS and the air, making its measurement crucial. Figures 3.8 and 3.9 present the schematic diagram and the actual experimental setup for measuring the interface current.

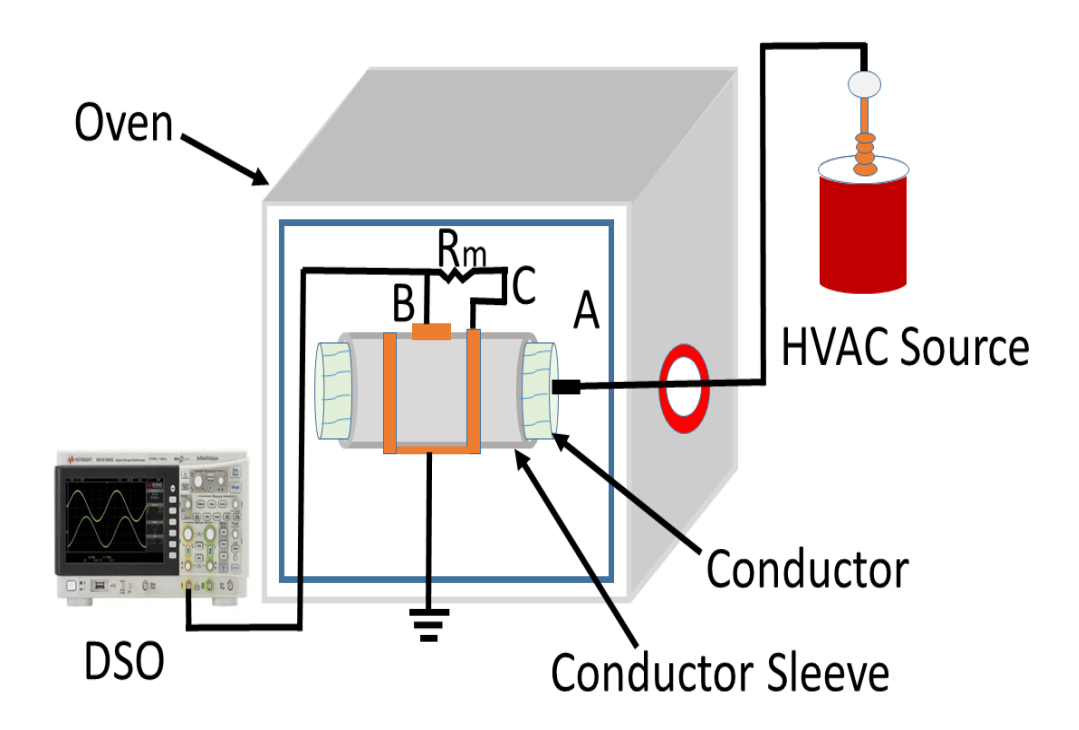


Figure 3.8 Schematic diagram for interface current measurement.

This experimental arrangement consists of three electrodes-the high-voltage (HV) electrode A, the rectangular shape, measuring electrode B and the guard electrode C is used. The dimensions of the measuring electrode and the gap between the guard and measuring electrodes is set according to the ASTM standard [33].

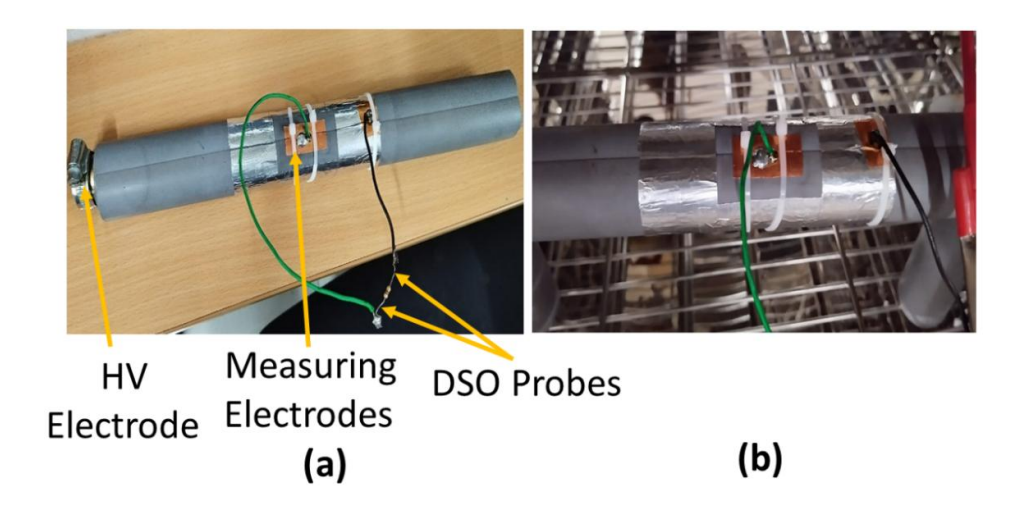


Figure 3.9 (a) Experimental setup for interface current measurement (b) measuring setup (inside oven view).

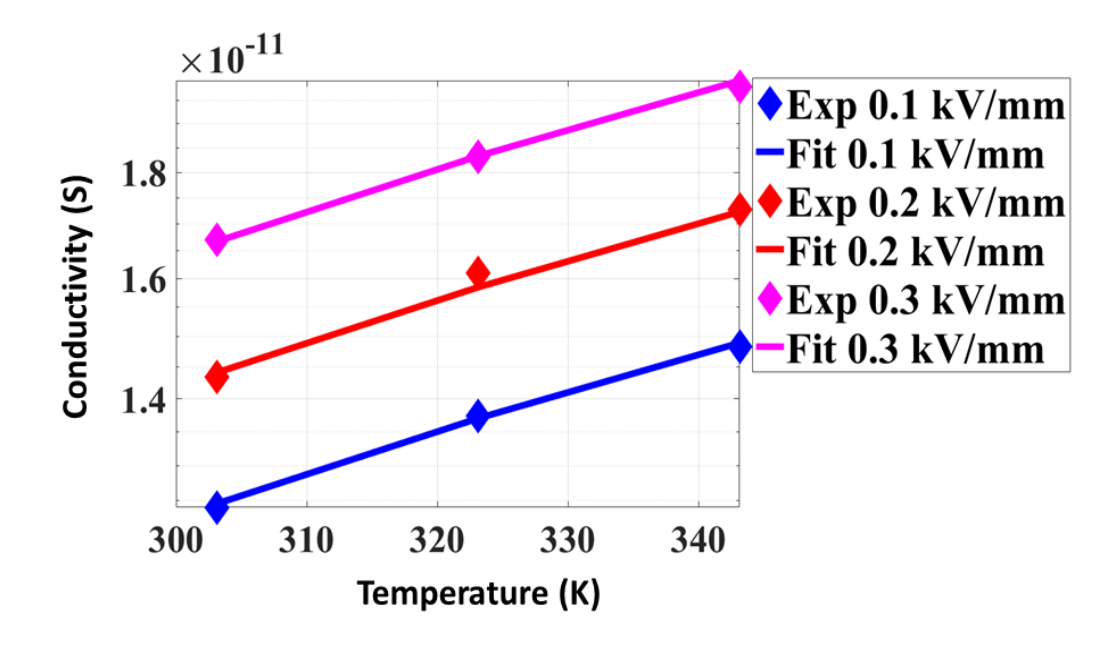


Figure 3.10 Interfacial ac conductivity of CS with respect to temperature and field: experimental and curve fitted.

To measure the interface current, the measuring electrode B is connected to the guard electrode C through a measuring resistor Rm with the terminals of Rm connected to a digital storage oscilloscope (DSO). The equivalent circuit for this measurement setup is identical to that used for surface current measurement (figure 3.5 (b)). The entire setup placed inside an oven (figure 3.9(b)), and experiments conducted at applied voltages of 1 kV, 2 kV, and 3 kV, with temperatures of 303.15 K, 323.15 K, and 343.15 K, respectively.

TABLE 3.4
Estimated interfacial coefficients of CS and goodness of fitting

Material	A	α	β	R^2	SSE
	(S)	(m/V)	(K)		
SCR	4.98×10 ⁻¹¹	1.46×10 ⁻⁶	464.2	0.99	0.0003

TABLE 3.5

Measured interfacial AC resistivity and conductivity for different voltages and temperatures

Volt	T	I	Ø	$ ho_{ m i}$	$\sigma_{\rm i}$
(V)	(K)	(μΑ)	(degree)	(Ω)	(S)
1000	303.15	70	83.6	8.055×10^{10}	1.241×10 ⁻¹¹
	323.15	69	82.8	7.277×10 ¹⁰	1.373×10 ⁻¹¹
	343.15	65	81	6.742×10 ¹⁰	1.483×10 ⁻¹¹
2000	303.15	74	80.1	6.973×10 ¹⁰	1.434×10 ⁻¹¹
	323.15	72.5	78.48	6.21×10 ¹⁰	1.61×10 ⁻¹¹
	343.15	68	77.4	5.625×10 ¹⁰	1.727×10 ⁻¹¹
3000	303.15	78	77.2	5.79×10 ¹⁰	1.672×10 ⁻¹¹
	323.15	74	73.8	5.46×10 ¹⁰	1.831×10 ⁻¹¹
	343.15	70	72	5.04×10 ¹⁰	1.983×10 ⁻¹¹

The various parameters computed and presented in table 3.5, following the same approach as in the case of surface current measurement. To determine the coefficients of equation (3.1), the measured data from table 3.5 used and applied least squares curve fitting. The resulting plot and the corresponding coefficients of equation (3.1) are shown in figure 3.10 and table 3.4, respectively. For the simulation process, the conductivity values measured on the surface (σ_s) and at the interface (σ_i) of the CS are converted into their corresponding volumetric conductivities. These are denoted as σ_{sv} for surface and σ_{iv} for interface, respectively by dividing with thickness of boundary layer (t) as per equation (3.9) and tabulated in table 3.6.

$$\sigma_{iv} = \frac{\sigma_i}{t}; \ \sigma_{sv} = \frac{\sigma_s}{t} \tag{3.9}$$

TABLE 3.6
Estimated volumetric conductivity of bulk, surface, and interface regions of CS at various temperatures and specific applied voltages

Volt	Т	$\sigma_{ m v}$	$\sigma_{ m sv}$	σ_{iv}
(V)	(K)	(S/m)	(S/m)	(S/m)
	303.15	8.88×10^{-10}	2.84×10 ⁻⁰⁸	6.21×10 ⁻⁰⁸
1000	323.15	1.29×10 ⁻⁰⁹	3.38×10 ⁻⁰⁸	6.87×10 ⁻⁰⁸
	343.15	1.74×10 ⁻⁰⁹	3.97×10 ⁻⁰⁸	7.41×10 ⁻⁰⁸

3.4 Analysis of Conductivity Variations and Their Implications

Table 3.6 to analyze the effects of temperature and electric field on bulk (σ_v) , surface (σ_{sv}) , and interfacial (σ_{iv}) conductivities of CS, their implications for dielectric behavior, and the rationale for observed trends. Table 3.6 reports conductivity values at 1000 V, standardizing bulk measurements (70 V, 700 V, 1050 V, Section 3.1) and surface/interfacial measurements (1000 V, 2000 V, 3000 V, Sections 3.2–3.3) for temperature of 303.15 K, 323.15 K, 343.15 K, at 50 Hz for 0.7 mm samples using a Novo-control Alpha-A analyzer. At 1000 V, bulk conductivity (σ_v) , rises from 10^{-10} S/m at 303.15 K to 10^{-9} S/m at 343.15K, driven by thermal activation (high β) as increased polymer chain mobility enhances ionic and electronic

transport. The electric field coefficient (α) is modest, with field-induced charge injection secondary to thermal effects. Surface (σ_{sv}), and interfacial (σ_{iv}) conductivities ($\sim 10^{-8}$ S/m) increase with temperature due to moisture, contaminants, and partial discharges. The bulk increase arises from intrinsic polymer mobility, whereas elevated σ_{sv} arises from surface states (e.g., absorbed moisture, dust, contamination etc.) and (σ_{iv}) from interfacial defects (e.g., micro-voids, filled with air caused moisture), amplified by electric field enhancement at the conductor-sleeve interface.

Elevated conductivity increases dielectric losses and thus promotes interfacial tracking and electro-thermal runaway. Higher conductivity identifies the interface as the primary site for tracking initiation due to localized discharges and field concentration. Novo-control's spectroscopy has a maximum limit of 1200 V constrained bulk measurements, but 1000 V enables consistent comparison.

The comparison of volumetric conductivities for the bulk, surface, and interface regions reveals that the interfacial region exhibits significantly higher conductivity than the other two, which may lead to initiate the tracking in the interfacial region. Further, the experimentally obtained parameters such as conductivity coefficient (A), electric field coefficients (α), and the temperature coefficient (β) of equation (3.1), have been integrated into the FEM software for simulations related to investigations of tracking and thermal runaway behaviour of CC and, CS, as discussed in the subsequent chapter.

3.5 Conclusions

This chapter details the experimental measurement of AC conductivity in CS, covering volumetric, surface, and interfacial regions. Novel setups were developed to measure surface and interfacial conductivity under varying temperatures and electric fields, revealing that interfacial conductivity is significantly higher, making it the primary site for tracking initiation. The results, validated through curve-fitting and tabulated in table 3.6, show that conductivity increases with temperature due to enhanced polymer mobility and environmental factors like moisture. These measurements provide critical parameters for FEM simulations, enabling accurate modeling of tracking and runaway phenomena, and highlight the importance of interfacial properties in CS performance.

FEM Modelling Analysis and Validation of CS Performance

This chapter provides a detailed analysis of CCs and CS modelled using FEM software to evaluate their electro-thermal performance. The study includes simulations under steady state rated conditions and transient scenarios, extending to the point of thermal runaway under various operating conditions. The simulation results were rigorously validated through experimental investigations, with details of the simulation model and a comprehensive discussion of the results presented.

4.1 Geometry, Material Properties and Simulation Model

The geometry of a medium-voltage (MV) CS with 180° and 90° overlapping angles, as illustrated in figure 3.1, is modelled using a 2-D FEM approach as depicted in figure 4.1. The CS features a conductor diameter of 26 mm and an overall diameter of 40 mm, with the insulation thickness in the interface region ranging from 7 to 10 mm.

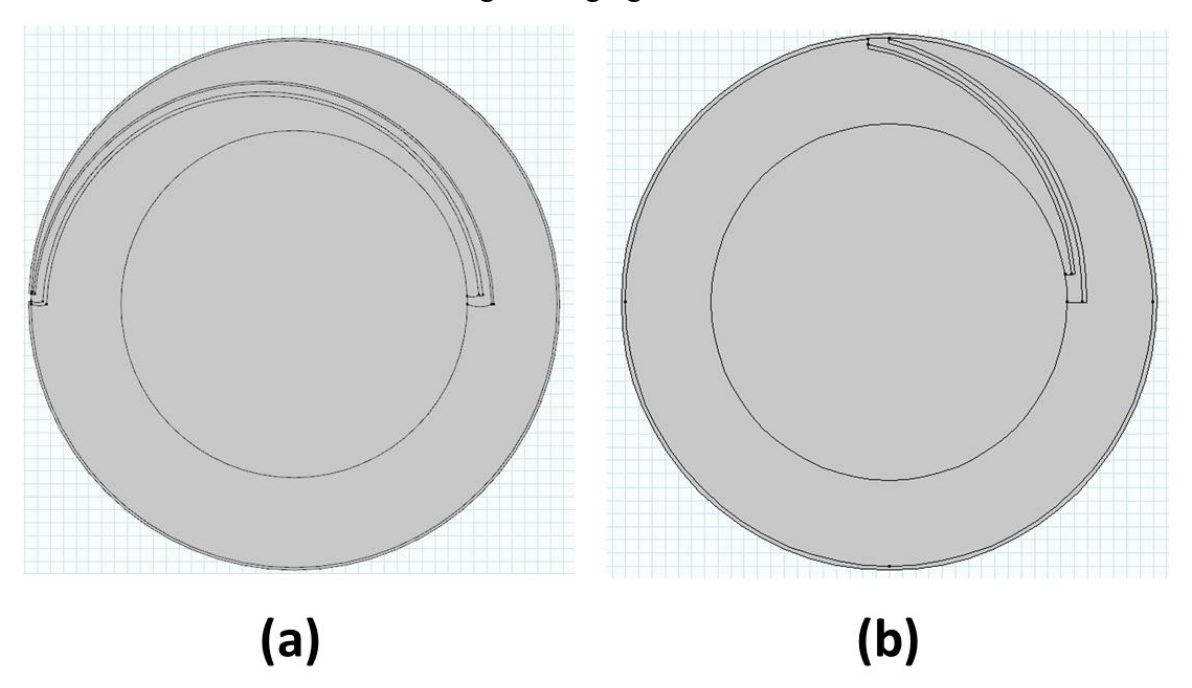


Figure 4.1 2-D simulation model of CS for (a) 180° overlapped (b) 90° overlapped configuration.

The model incorporates key parameters such as relative permittivity, volumetric AC conductivity (measured through dielectric spectroscopy), and surface and interfacial AC conductivity (determined using the setup described in the previous chapter). The relative

permittivity was measured to be 2.3 under the conditions outlined in [34]. Additionally, the model accounts for the non-linear behavior of AC conductivity.

A triangular mesh with an extremely fine element size (less than 0.5 mm) was used to ensure high accuracy in the simulation results. The mesh was sufficiently refined to reliably capture the necessary field variations. Neumann boundary conditions were applied to model the flux or field variables at the boundaries, ensuring accurate physical representation. A mesh independence study confirmed that the results were stable and independent of further refinement.

The dimensional details of the model and other relevant parameters are provided in table 4.1. The research also investigates the impact of overlapping angles in conductor sleeves (CS) and evaluates their comparative performance in terms of electro-thermal instability.

TABLE 4.1 Simulation Model Parameters

Parameters	Numerical Values	Units
Total CS diameter	40	mm
Conductor diameter	26	mm
Insulation thickness	7	mm
Relative permittivity	2.3	
Initial temperature	293.15	K
Air conductivity	1.5×10 ⁻¹²	S/m

4.2 Governing equations:

The Computations of the electric field, current density distribution, and temperature profile within the CS geometry involves solving coupled differential equations, namely the current continuity equation and the heat continuity equation, along with other field-related equations. Under steady-state conditions, the current continuity equation, which encompasses all four of

Maxwell's equations [35], states that the net rate of charge accumulation or depletion within a given volume is zero. This can be mathematically expressed as follows:

$$\nabla \cdot J = 0 \tag{4.1}$$

Where, J is total current density, and it can be expressed as

$$J(t) = J_C(t) + J_D(t)$$
(4.2)

Here, $J_C(t)$ represents the conduction current density. Since this study primarily examines alternating current (AC) fields, the magnitude of $J_C(t)$ is minimal and is therefore, neglected for simplification. As a result, the total current density is considered equal to the displacement current density $J_D(t)$.

Given that the present study focuses on AC fields (alternating current), the magnitude of $J_C(t)$ being very small, is thus neglected for simplification. Consequently, the total current density is equivalent to the displacement current density $J_D(t)$;

$$J(t) = J_D(t) = \frac{\partial D(t)}{\partial t}$$
(4.3)

Where, D(t) is the electrical flux density, expressed as

$$D(t) = \varepsilon_0 \varepsilon_r E(t) = \varepsilon_0 (\varepsilon_r' - j\varepsilon_r'') E(t)$$
(4.4)

Further, the equation (4.3) becomes

$$J(t) = \frac{\partial D(t)}{\partial t} = \frac{\partial \varepsilon_0(\varepsilon_r' - j\varepsilon_r'')E(t)}{\partial t}$$
(4.5)

In frequency domain, equation (4.5) can be expressed as

$$J(\omega) = j\omega \varepsilon_0(\varepsilon_r' - j\varepsilon_r'')E(\omega) \tag{4.6}$$

Where, ω is the angular frequency, rearranging the equation we get

$$I(\omega) = j\omega\varepsilon_0\varepsilon_r'E(\omega) + \omega\varepsilon_0\varepsilon_r''E(\omega) \tag{4.7}$$

The expression obtained in the above equation comprises both real and imaginary

components. The real component contributes to power loss, while the imaginary component contributes to stored energy. The term $\omega \varepsilon_0 \varepsilon_r''$ is commonly known as AC conductivity as expressed in equation (2.2).

Further utilizing equation (2.2) and (3.1), AC conductivity can be expressed as

$$\sigma = \omega \varepsilon_0 \varepsilon_r^{"} = A e^{\alpha E - \frac{\beta}{T}} \tag{4.8}$$

Whereas the relationship between the electric field E and voltage V arises from the well-known field equation, given by

$$\mathbf{E} = -\Delta . V \tag{4.9}$$

(4.7), (4.8) and (4.9) depict the relation of electric field, current density and temperature. The thermal continuity equation within dielectric layers can be expressed as the balance between the heat generated, heat accumulation, and heat dissipated. The associated equation describing this relationship is as follows:

$$DC_{p} \frac{\partial T}{\partial t} - \nabla \cdot (k\nabla T) = JE(t) = \sigma E(t)^{2}$$
(4.10)

Where, D, C_p , k, T are the density, heat capacity at constant pressure, thermal conductivity and temperature respectively.

If I_L is the load current, R_C is the conductor resistance per unit sleeve length, r_1 is the conductor radius and k is the insulation thermal conductivity, then, as per Fourier's law,

$$q = -k\Delta T = \frac{I_L^2 R_c}{2\pi r_1} \tag{4.11}$$

Here, q, ΔT denote heat flux density & temperature gradient.

4.3 Analysis and Interpretation of Simulation Results

The initial analysis includes simulating the CS under rated operating conditions. Furthermore, scenarios were examined, where a tree branch approached the CS, with the worst-case scenario involving direct contact between the tree branch and the conductor sleeve.

At the rated voltage (11kV), the highest electric field within the interface region found near the innermost layer, adjacent to the conductor surface, as in figure 4.2 and 4.3 illustrated.

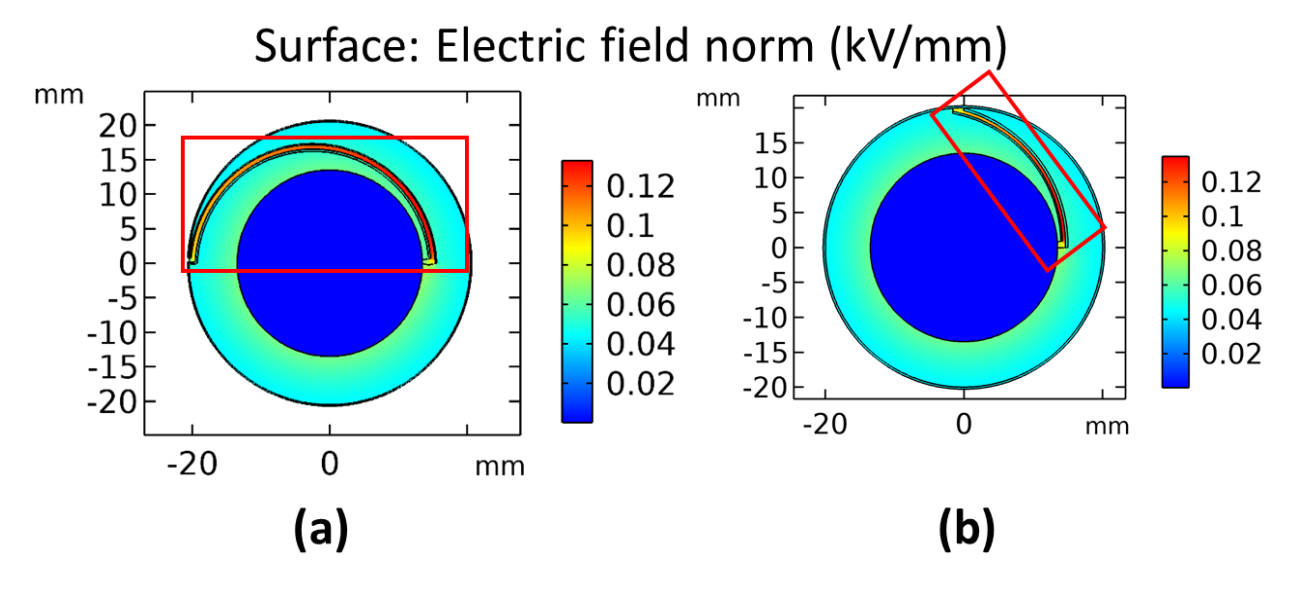


Figure 4.2 Electric field distribution at rated voltage for (a) 180° overlapped (b) 90° overlapped configuration

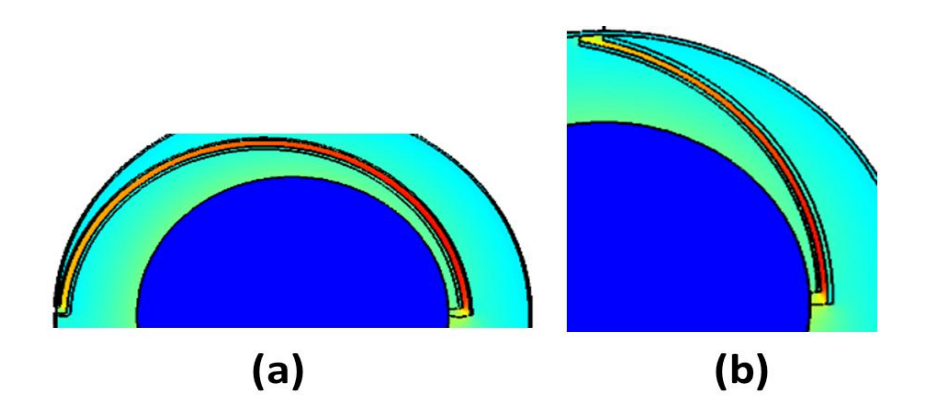


Figure 4.3 Enlarged view of selected area of figure 4.2.

The relationship between current density and electric field, as described by equation (4.7), shows a direct correlation. The current density distribution was observed similar to the electric field distribution, as shown in figure 4.4. Due to the variation in current density between the conductor and insulation, the current distribution is specifically depicted only within the interface region in figure 4.4.

The investigation further examines the scenario where a tree branch, treated as a ground electrode, makes direct contact with the surface of the CS specifically when the ground electrode is placed at the outermost edge of the interface, adjacent to the CS surface. The

simulated electric field and current density distribution profiles for this scenario are presented in figures 4.5 and 4.6. Additionally, simulations were conducted for cases where the ground electrode is positioned at various distances from the CS surface.

Surface: Current density $norm(A/m^2)$

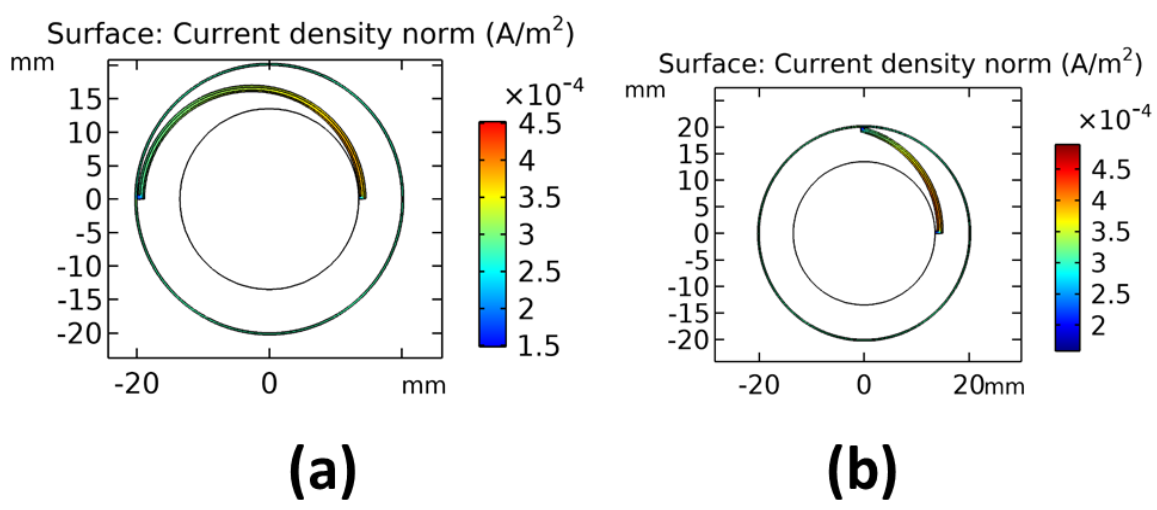


Figure 4.4 Current density distribution at rated voltage for (a) 180° overlapped (b) 90° overlapped configuration.

Surface: Electric field norm (kV/mm)

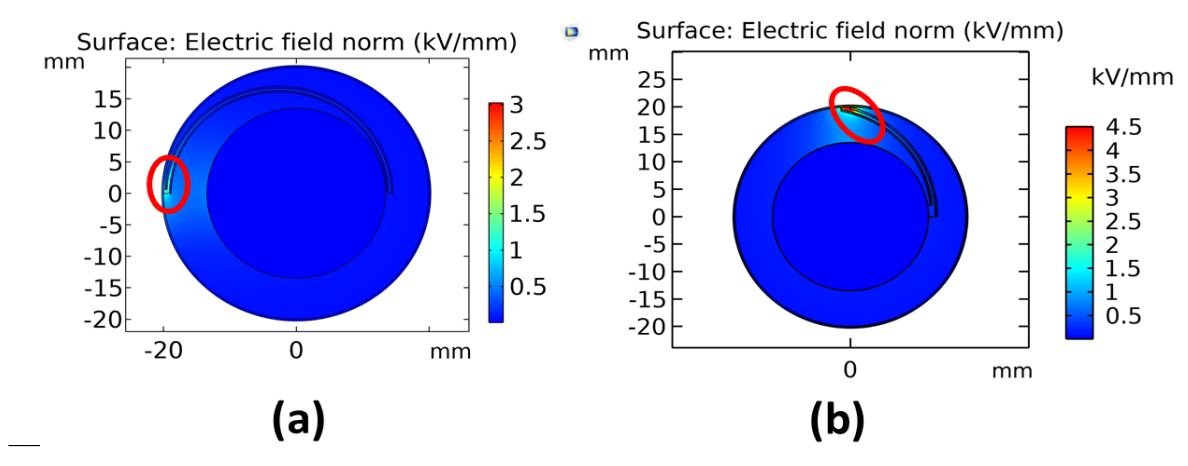


Figure 4.5 Electric field distribution at rated voltage, in case of tree branch touching the CS surface for (a) 180° overlapped (b) 90° overlapped configuration

The peak electric field and current density within the interface region are summarized in table 4.2 and illustrated in Figures 4.7 (a) and (b), respectively. The results clearly show that the highest electric field and current density occur when there is direct contact with the conductor sleeve. In contrast, as the distance between the ground electrode and the CS surface increases,

both the electric field and current density decrease in magnitude, as depicted in figure 4.7. Therefore, the direct contact scenario is identified as the worst-case condition.

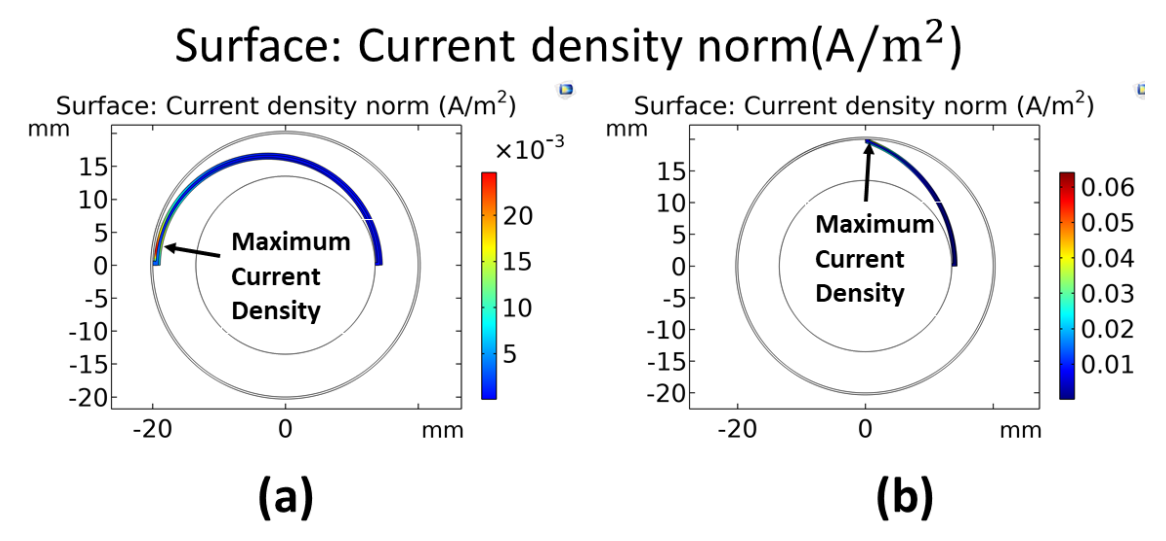


Figure 4.6 Current density distribution at rated voltage, in case of tree branch touching the CS surface for (a) 180° overlapped (b) 90° overlapped configuration.

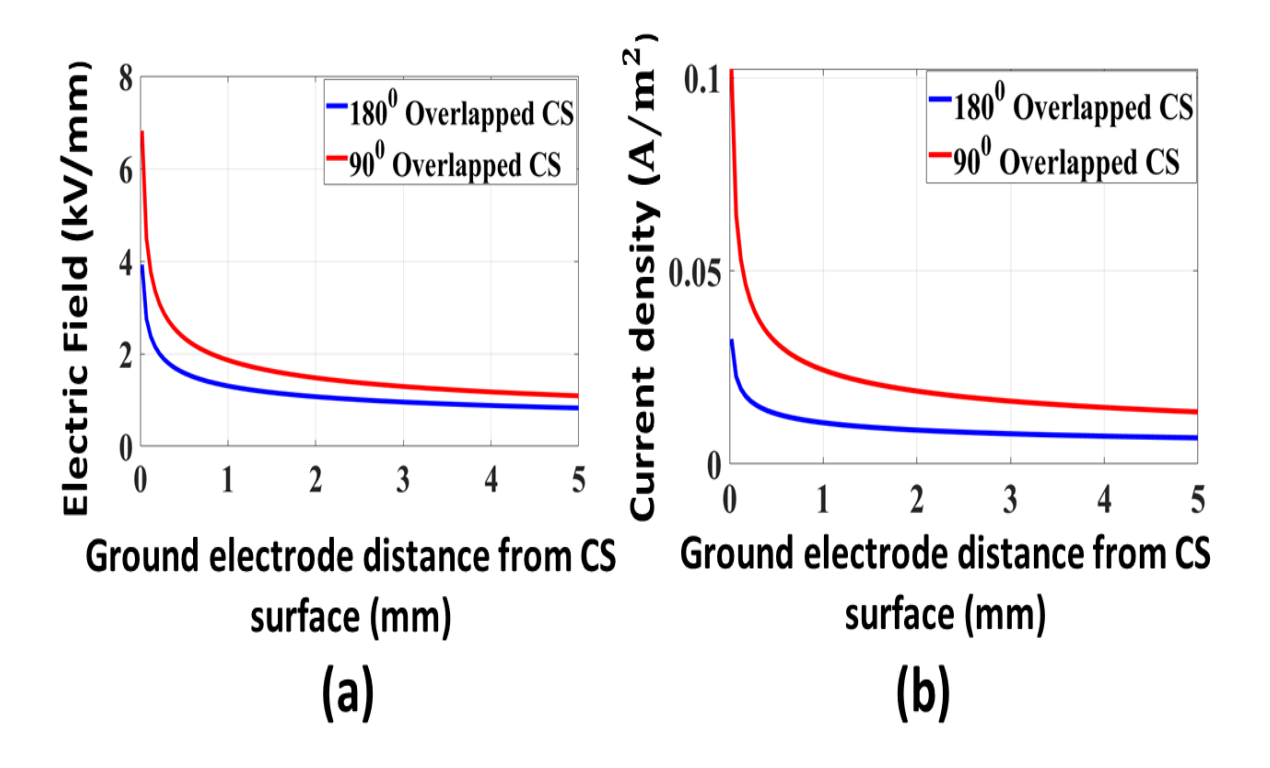


Figure 4.7 (a) Peak electric field and (b) current density relative to ground electrode distance from CS surface.

TABLE 4.2
Peak electric field and current density in the interface of CS at rated voltage

Ground	180° ov	erlapped	90° overlapped		
electrode position from CS surface (mm)	Electric field (kV/mm)	Current density (A/m²)	Electric field (kV/mm)	Current density (A/m²)	
0	3.40	0.0265	5.11	0.07	
0.5	1.96	0.0169	3.56	0.05	
1	1.53	0.013	2.43	0.033	
1.5	1.27	0.0109	1.97	0.027	
2	1.12	0.0096	1.64	0.022	
2.5	0.96	0.0084	1.40	0.019	
3	0.89	0.0075	1.16	0.015	
3.5	0.85	0.0069	1.13	0.0138	
4	0.83	0.0065	1.01	0.0119	
4.5	0.79	0.0060	0.96	0.0109	
5	0.78	0.0059	0.89	0.0098	

It is important to note that the location of the peak electric field changes depending on the operating conditions. Under normal operation (without a nearby ground), the peak field is observed near the innermost layer of the interface region. However, when a ground electrode is present, the peak field shifts toward the outermost layer of the interface, close to the CS surface. Additionally, an interesting finding concerns the overlapping angle. The maximum electric field and current density are significantly higher (as depicted in figure 4.7) in the 90° overlapped CS. This could suggest a faster rate of material degradation, which may exacerbate thermal instability in the 90° overlapped CS configuration.

To model electro-thermal runaway, additional time-domain simulations were carried out. In these simulations, the ground electrode was placed at distances of 0 mm (i.e., directly on the CS surface), 1 mm, 2.5 mm, and 5 mm from the CS surface, for various applied voltages. Simulations were conducted under no load and performed until runaway occurred at a specific voltage, referred to as the simulated interface tracking inception voltage (ITIVsim). The corresponding times for the initiation of runaway were recorded for each case.

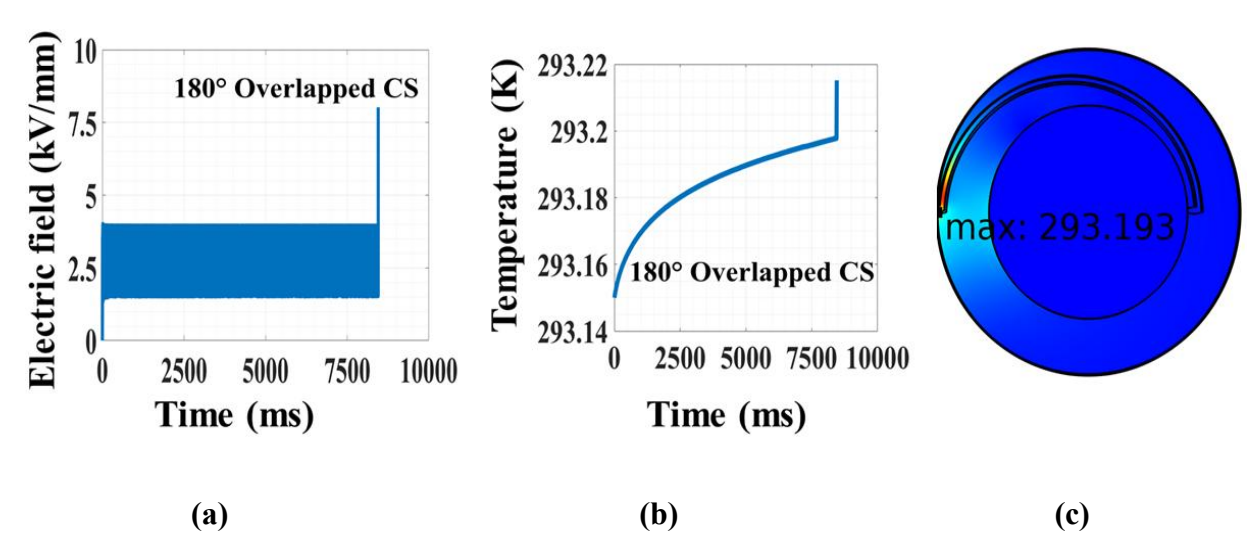


Figure 4.8 Runaway in 180° CS (a) Electric field (b) Temperature and (c) Field distribution.

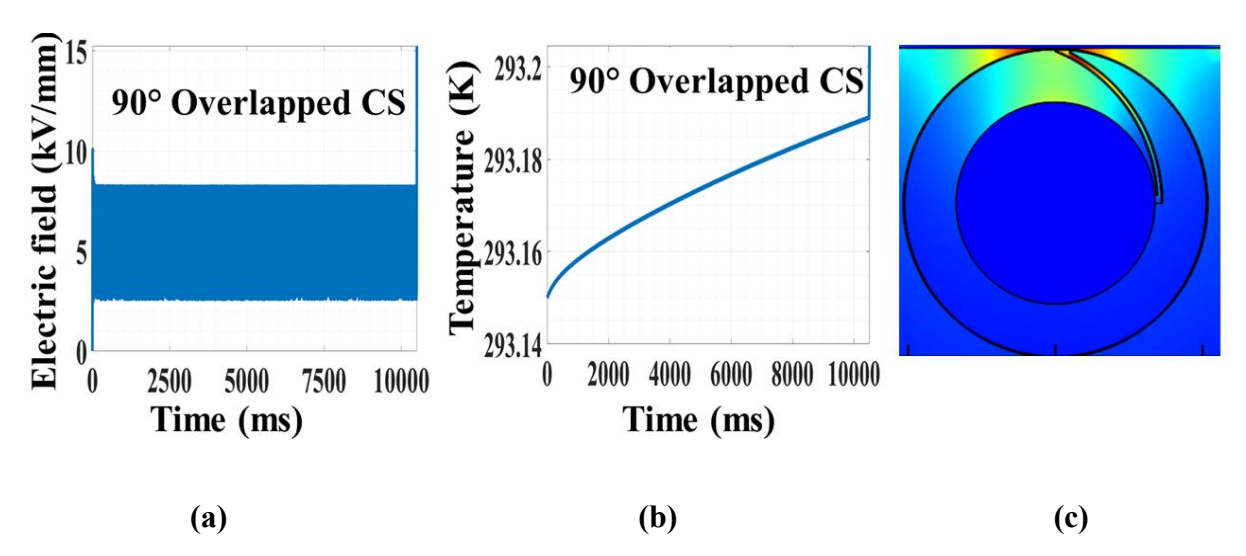


Figure 4.9 Runaway in 90° CS (a) Electric field (b) Temperature and (c) Field distribution.

It was observed that after a certain threshold time, instability is triggered in the interfacial region, as shown in figure 4.8 and 4.9 (when a tree branch touches the CS surface). This phenomenon can be attributed to the increased equivalent interfacial volumetric conductivity, as indicated in table 3.6.

The time at which runaway occurs is referred to as the time to breakdown. It was observed that, beyond a certain threshold time, instability is triggered in the interfacial region, as shown in figure 4.8 and 4.9 (when a tree branch makes contact with the CS surface, i.e., the ground electrode touches the outermost tip of the CS surface). Once the thermal breakdown mechanism is triggered, it leads to an uncontrolled rise in both temperature and electric field, creating a singularity. This occurs mainly due to a sudden increase in the AC conductivity of the interface, which initiates an internal cascading effect, ultimately resulting in runaway. Figure 4.8 and 4.9 show simulations conducted at higher voltages to observe runaway within a finite computational timeframe. However, since the time to runaway decreases with increasing voltage [36], at rated voltage, runaway is expected to take significantly longer to initiate.

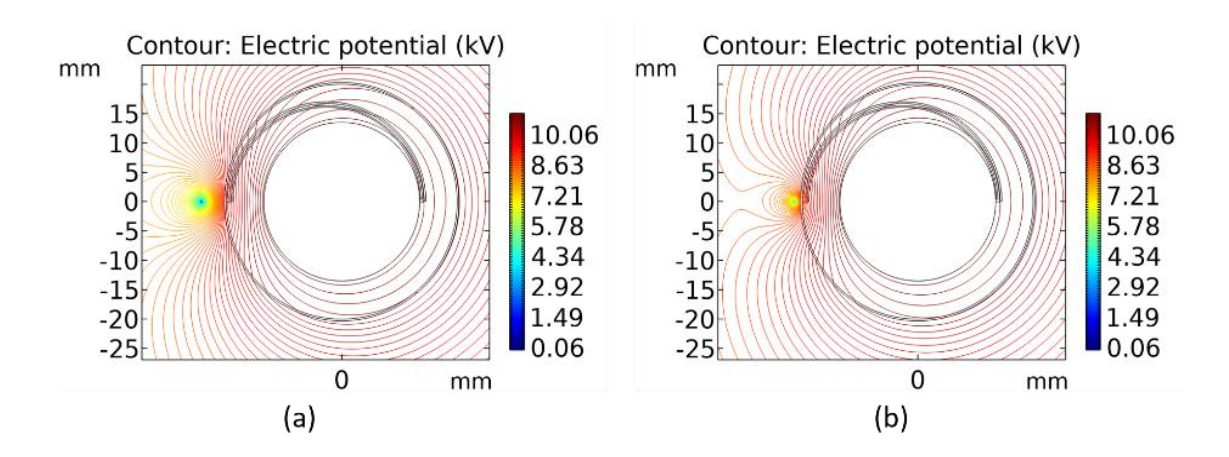


Figure 4.10 Equipotential line distribution in 180°CS for (a) 5mm and (b) 1mm distance from surface.

Furthermore, it has been observed that positioning the ground electrode near the outermost edge of the CS interface surface results in the highest electric field intensity and current density. Conversely, as the ground electrode is moved further away from the CS surface, both the electric field intensity and current density gradually decrease, the occurrence of this phenomena is due to the location of the point ground electrode significantly impacts the distribution of equipotential lines. When positioned farther from the sleeve surface, such as at a distance of 5 mm, the equipotential lines appear more spread out, as illustrated in figure 4.10 (a), leading to a reduction in both electric field intensity and current density. Conversely, as the electrode kept closer to the surface, at 1 mm for instance, the lines become more concentrated, as depicted in figure 4.10 (b), causing an increase in the electric field. The most

critical scenario arises when the point ground makes direct contact with the surface, resulting in maximum field enhancement.

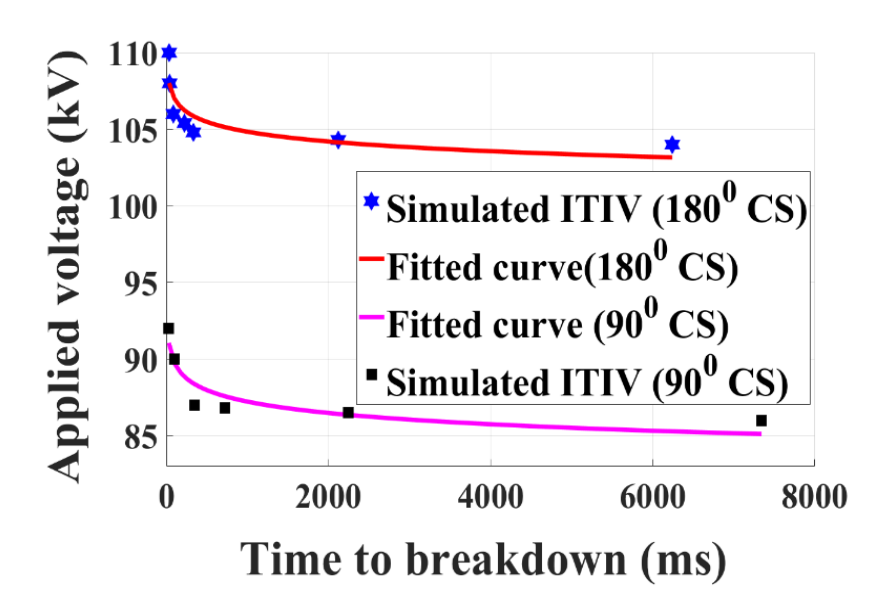


Figure 4.11 V-t characteristics for 5 mm ground electrode distance from CS surface.

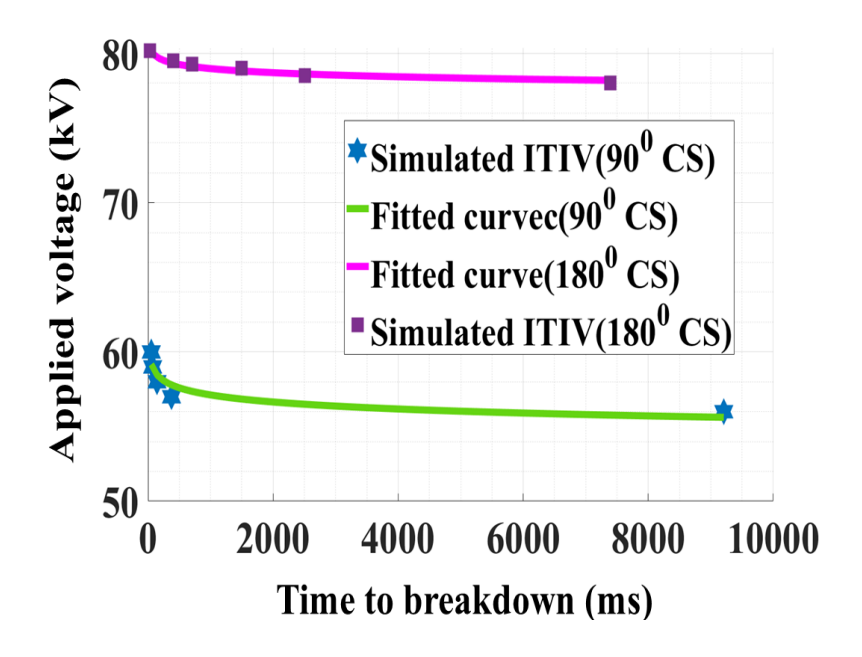


Figure 4.12 V-t characteristics for 2.5 mm ground electrode distance from CS surface.

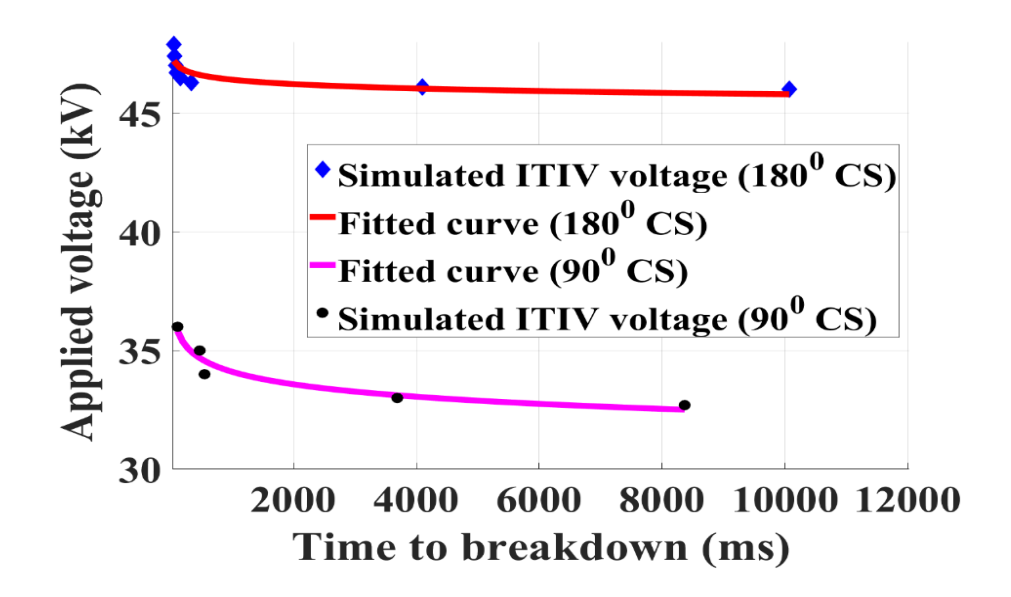


Figure 4.13 V-t characteristics for 1 mm ground electrode distance from CS surface.

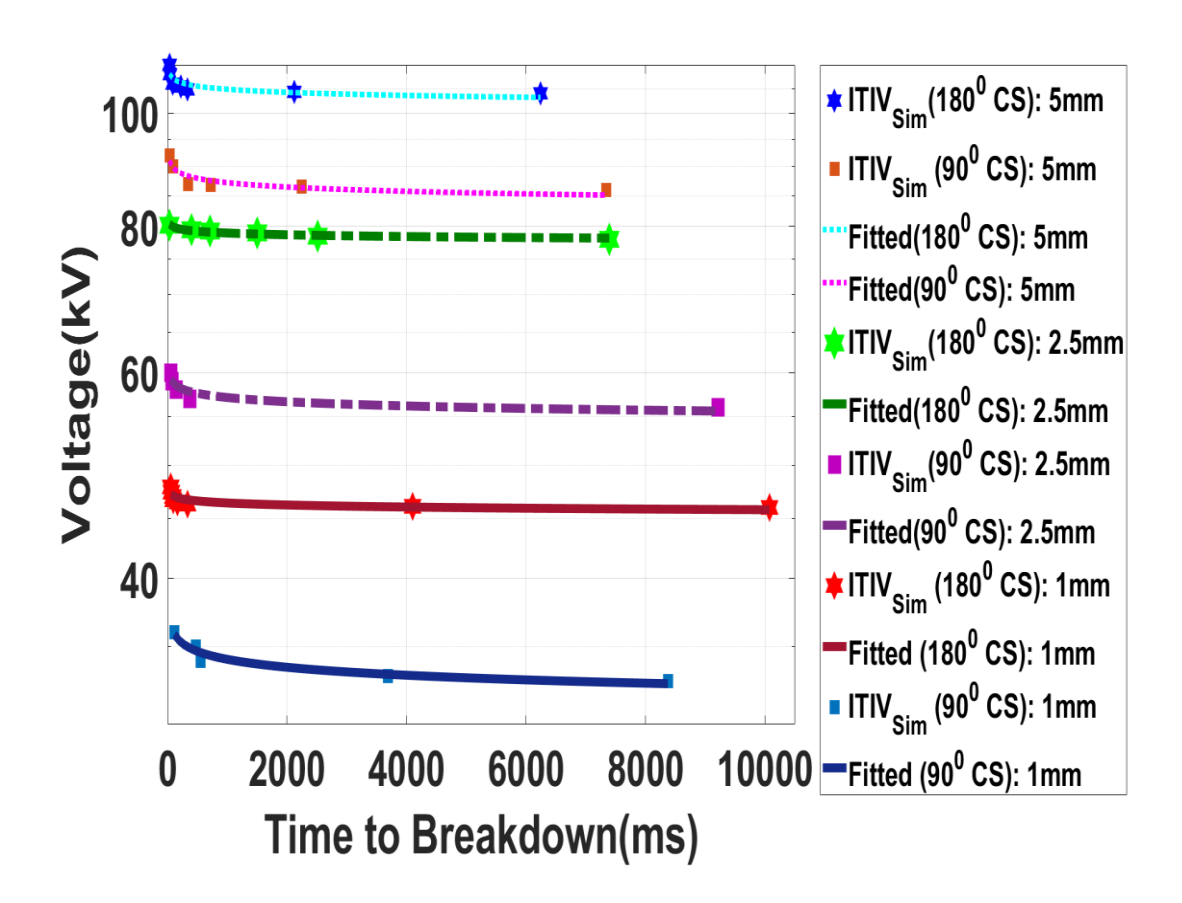


Figure 4.14 V-t characteristics for ground electrode at 5mm, 2.5mm, and 1mm from CS surface.

The correlation between the applied voltage and the time to electrical runaway, often referred to as the V-t characteristics, was evaluated for both 180° and 90° conductor sleeve (CS) configurations at varying distances of the ground electrode from the CS surface. These

relationships are illustrated in figure 4.11 to 4.13, while figure 4.14 provides a consolidated view of the V-t characteristics for ground electrode distances of 5 mm, 2.5 mm, and 1 mm from the CS surface. The simulated data points were analysed using an inverse power law model, as detailed in [37-38], a method commonly employed in electrical insulation research to describe material behaviour under prolonged high-voltage stress.

The analysis indicated a pronounced decrease ITIVsim as the ground electrode was positioned closer to the CS surface. This reduction is attributed to the elevated electric field intensity near the insulation due to the electrode's proximity, resulting in increased stress on the material. This behaviour was consistently observed across all tested configurations, underscoring the critical influence of the electrode's distance from the CS surface on ITIVsim.

Furthermore, the 90° overlapped CS configuration consistently exhibited lower ITIVsim values compared to the 180° overlapped CS. This disparity arises from the more concentrated electric field intensity in the 90° configuration. The reduced overlap in the 90° CS design results in localized regions of intensified field stress, which weaken the insulation's performance and heighten the risk of dielectric breakdown.

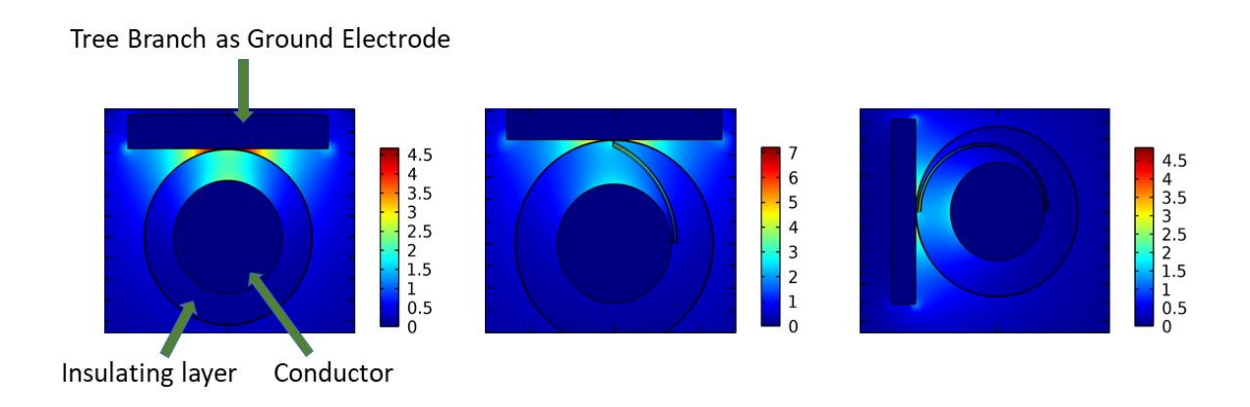


Figure 4.15 Electric field distribution at rated voltage in the (a) CC (b) 90° overlapped CS (c) 180° overlapped CS.

These results highlight the significant role of geometric design in determining the performance of conductor sleeves. For applications that demand higher ITIVsim and greater reliability, the 180° overlapped CS demonstrates superior performance. In contrast, although the 90° configuration may provide certain design advantages in specific applications, its diminished ability to manage field stress requires careful consideration, especially when the ground electrode is positioned close to the CS surface.

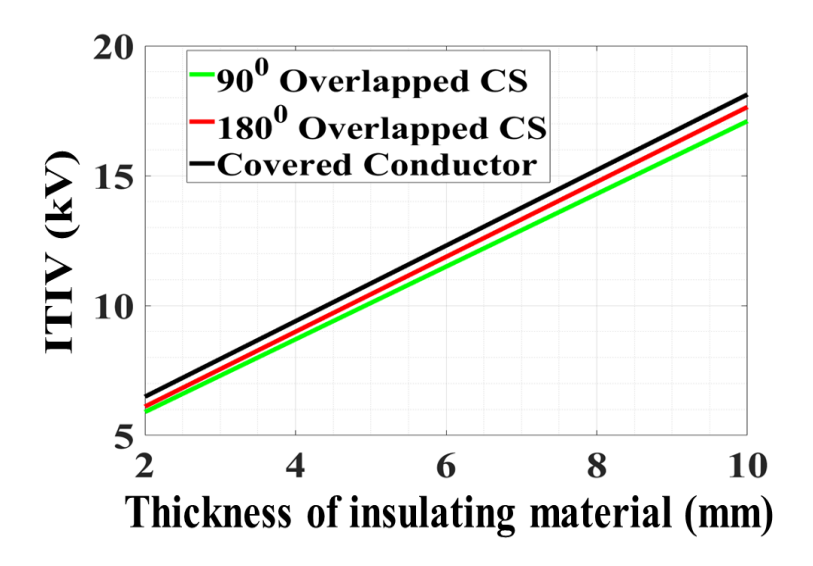


Figure 4.16 ITIV_{Sim} Vs. insulation thickness for CC, 90° and 180° overlapped CS.

CS and CCs exhibit comparable construction and functionality, making a comparative study necessary. A fault scenario was modelled, simulating a tree branch in contact with the surface of both CCs and CS, leading to an increased contact area, as shown in figure 4.15. The corresponding ITIVsim were evaluated, with the outcomes presented in figure 4.16. The analysis revealed that ITIVsim consistently increased with thickness across all cases. Although CCs demonstrated slightly higher ITIVsim values than CS, the difference was relatively small. This highlights the advantages of CS, including better adaptability to geographic challenges and enhanced reusability, making them a favourable choice over CCs. Moreover, the study showed that 180° overlapped CS performs better than 90° overlapped CS for the same thickness. To achieve comparable ITIVsim to a 180° overlapped CS, a 90° overlapped CS would require an increase in thickness, as illustrated in figure 4.16.

4.4 Analysis and Validation of Tracking Inception Voltage in Insulated Conductor Systems

An experimental setup as depicted in figure 4.17 was designed to align with the simulation results and determine the experimental inception tracking voltage (ITIVExp) for CCs and CS. This voltage represents the point at which tracking begins. In the setup, a CS is wrapped around a solid conductor and positioned at a defined height. The point ground electrode's distance from the sleeve surface is adjusted between 0 mm and 5 mm. Additionally, a corona ring is incorporated to prevent unintended flashovers.

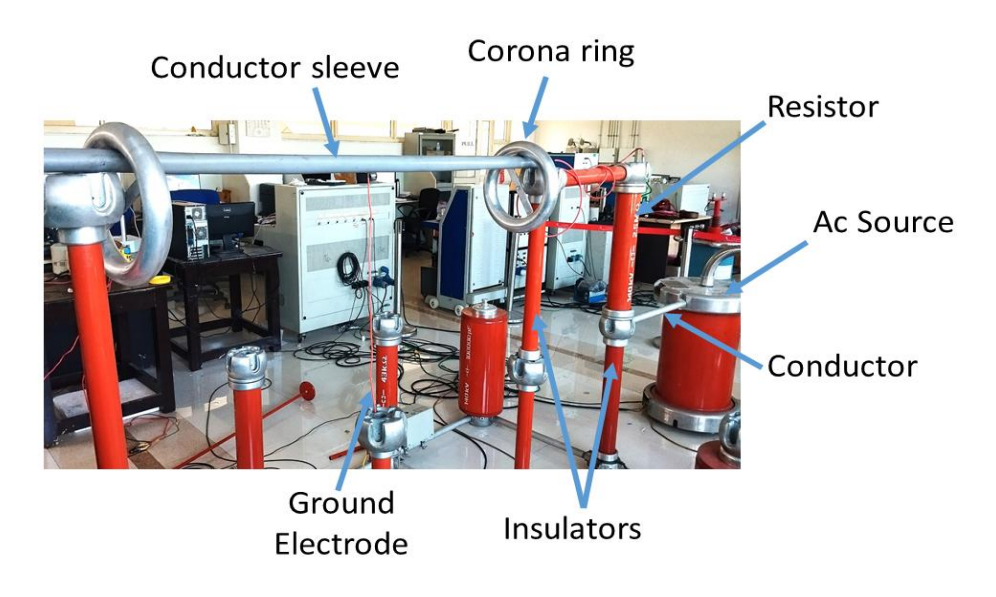


Figure 4.17 Experimental setup for estimation of ITIV.

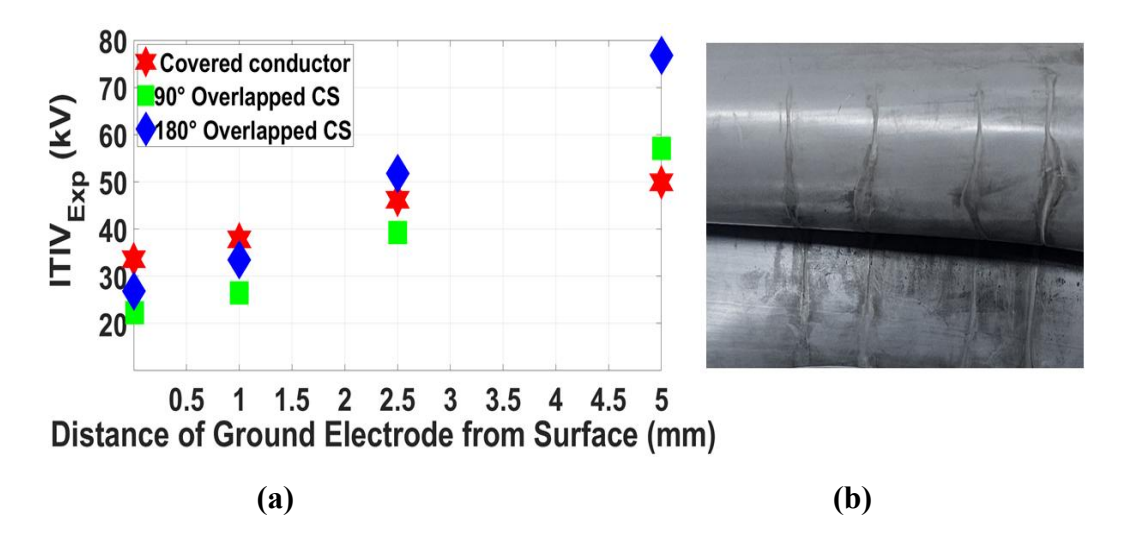


Figure 4.18 (a) $ITIV_{Exp}$ characteristics of CC and CS and (b) Surface tracking path formation.

When the ground electrode is positioned away from the surface, a notable reduction in ITIV for CC is observed in comparison to CS, despite both being designed for the same voltage ratings. This behaviour highlights differences in the dielectric performance of the two configurations under tracking conditions. The experimental observations reveal that surface-tracked paths in the CS interface are often accompanied by carbon deposition and arc initiation, as depicted in figure 4.18(b). These paths provide evidence of progressive degradation mechanisms, where localized heating and material erosion contribute to carbonization.

TABLE 4.3
Comparison of tracking inception voltage with the runaway inception voltage in the interface of CS & CC surface

Ground electrode position from	180° overlapped CS		90° overlapped CS		Covered conductor (CC)	
surface of CC & CS (mm)	ITIV _{Exp} (kV)	ITIV _{Sim} (kV)	ITIV _{Exp} (kV)	ITIV _{Sim} (kV)	ITIV _{Exp} (kV)	ITIV _{Sim} (kV)
0	26.85	13.40	22.25	13.05	33.6	13.85
1	33.5	43.30	28.00	33.50	37.8	45.2
2.5	51.8	78.20	39.30	57.80	46.2	54.85
5	76.8	105.3	52.10	87.80	49.85	84.35

The discrepancies between ITIV_{exp} (measured experimentally) and ITIV_{sim} (derived through simulations) can be attributed to the inherent differences between tracking and runaway phenomena. While both are closely related, tracking pertains to the initial development of conductive paths on the surface due to localized discharges, whereas runaway refers to the escalation of these paths into sustained arcing. These differences result in variations in onset conditions and intensities, making the observed increasing trends in both ITIV metrics particularly significant for understanding the material behaviour and improving design reliability.

It is essential to emphasize the significance of the observed trends. Both ITIV_{exp}, and ITIV_{sim} exhibit a consistent increase as the distance of the ground electrode from the sleeve surface is increased (as presented in table 4.3). This relationship highlights a strong correlation between the tracking and runaway phenomena, indicating that the initiation and progression of surface discharges are influenced by the proximity of the ground electrode.

From (figure 4.18 (a)), the analysis of the results, it can be inferred that the 180° CS configuration offers significant advantages over the CC and 90° CS designs. The 180° CS not

only exhibits higher ITIV values but also demonstrates improved resistance to surface tracking and carbon deposition under varying operational conditions. These advantages make the 180° CS a more reliable choice for practical applications, particularly where higher dielectric integrity and enhanced performance are required. The findings further suggest that, despite the challenges posed by practical operational constraints, the 180° CS strikes a better balance between performance and feasibility, positioning it as a promising solution in medium-voltage transmission systems.

4.5 Limitations of the Simulation Model and Discrepancy Analysis:

The FEM model demonstrates high accuracy under conditions where the ground electrode is positioned at greater distances (1 mm to 5 mm), as evidenced by the closer alignment between ITIV_{sim} and ITIV_{exp} in table 4.3. The model effectively capturing the electro-thermal dynamics of CS and CC under steady-state and transient conditions, validated by the consistent increasing trend of ITIV with increasing electrode distance. The use of measured parameters, such as volumetric, surface and, interfacial AC conductivity (table 3.6), and the incorporation of governing equations (Section 4.2) ensure robust modelling of field and thermal interactions. However, the position of the point ground (0 mm) electrode alters the distribution of the equipotential lines. When it is far away from the sleeve surface, the lines tend to be relaxed, leading to a lower electric field and current density. On the contrary, as it moves closer to the surface, the lines start getting concentrated, with the worst-case scenario being the point ground touching the surface. The 2-D FEM approach simplifies the geometry and assumes isotropic material behaviour, which may not fully represent the three-dimensional complexities of surface tracking at direct contact.

4.6 Conclusions

This Chapter presented a comprehensive analysis of conductor sleeves (CS) and covered conductors (CC) through finite element method (FEM) modelling, focusing on their electrothermal performance under steady-state and transient conditions. The study evaluates the impact of overlapping angles (90° and 180°) on tracking and electro-thermal runaway phenomena, validated through experimental measurements of interface tracking inception voltage (ITIV). Key findings include the superior performance of the 180° overlapped CS, which exhibits higher ITIV values compared to the 90° overlapped CS and CC, attributed to reduced electric field intensity and enhanced dielectric stability. The FEM simulations reveal that peak electric field and current density are maximized at direct contact (0 mm ground

electrode distance), decreasing with greater separation (Figures 4.7(a) and (b)). The 90° CS configuration shows higher susceptibility to tracking due to concentrated field stress, suggesting that increased insulation thickness could improve its performance (Figure 4.16). Experimental validation confirms the simulation trends, with ITIV_{exp} increasing as the ground electrode distance grows (table 4.3). However, discrepancies at 0 mm, where ITIV_{sim} is significantly lower than ITIV_{exp}, highlight limitations in the 2-D FEM model. These differences stem from field non-uniformity, surface condition variability, and unmodeled material property variations, which are more pronounced at direct contact. The model's accuracy is higher at greater distances, where assumptions of uniform fields and material properties align more closely with experimental conditions. The analysis underscores the critical role of geometric design in enhancing CS reliability. The 180° overlapped CS is recommended for medium-voltage applications due to its robust performance and adaptability. Future improvements to the simulation model, including 3-D modelling and dynamic surface conditions, could address the observed discrepancies and further refine the understanding of tracking and runaway mechanisms.

Chapter 5

Impact of Load Current on the Performance of Conductor Sleeves

The investigations presented until now were dedicated to understanding the electro-thermal modelling and tracking inception voltage in CS, largely based on insulation's intrinsic dielectric properties. It is, however, imperative, that the performance of CS is also dependent on external factors such as load current through the conductor.

The performance and durability of conductor sleeves significantly influenced by variations in load current, which imposes thermal, electrical, and mechanical stresses. High load currents can lead to overheating, causing material degradation and reducing structural integrity. On the other hand, under-current conditions may result in inefficient energy utilization or insufficient stress testing. These fluctuations can affect the reliability and lifespan of conductor sleeves, necessitating their consideration during design, installation, and maintenance.

Manufacturers must carefully analyse the effects of load current variations during the design phase. Evaluating parameters such as temperature rise, electrical conductivity, and mechanical stability ensures that the sleeves can withstand a range of operational conditions. Advanced simulation tools and the use of optimized materials are vital for developing robust designs capable of addressing these challenges. Proper installation practices are equally important to maintain sleeve performance under varying load conditions. Secure fittings, precise alignment, and adherence to installation standards are critical to avoiding issues such as thermal expansion, misalignment, or loose connections.

The flow of load current through a conductor generates heat, with the heat output proportional to the square of the current. This heat is transferred to the conductor sleeve, creating a temperature gradient between the conductor and the sleeve material. Increased load currents can elevate temperatures beyond design limits, leading to thermal aging of the sleeve material. Over time, this degrades the mechanical strength and dielectric properties of the sleeve, compromising its effectiveness. Additionally, thermal expansion and contraction caused by fluctuating load currents can exacerbate material degradation, potentially resulting in cracks or delamination.

Thus, in this chapter, the discussion is mainly focused on the experimental analysis to analyse the performance of CS, based on load current variation, which is further validated with simulation for a specific case. In addition, the author investigates a remedial measure to increase the ITIV of CS. Based on a rigorous evaluation; it was found that the use of an additional insulation tape might prove to be effective, which is elaborated in the following sections. Thus, the following two cases are discussed: CS without insulation tape and with insulation tape.

5.1 CS without insulation tape:

The schematic and actual experimental setup are shown in figure 5.1 and 5.2 was developed to investigate the effect of temperature rise due to the rise of load current on the tracking phenomena of CS.

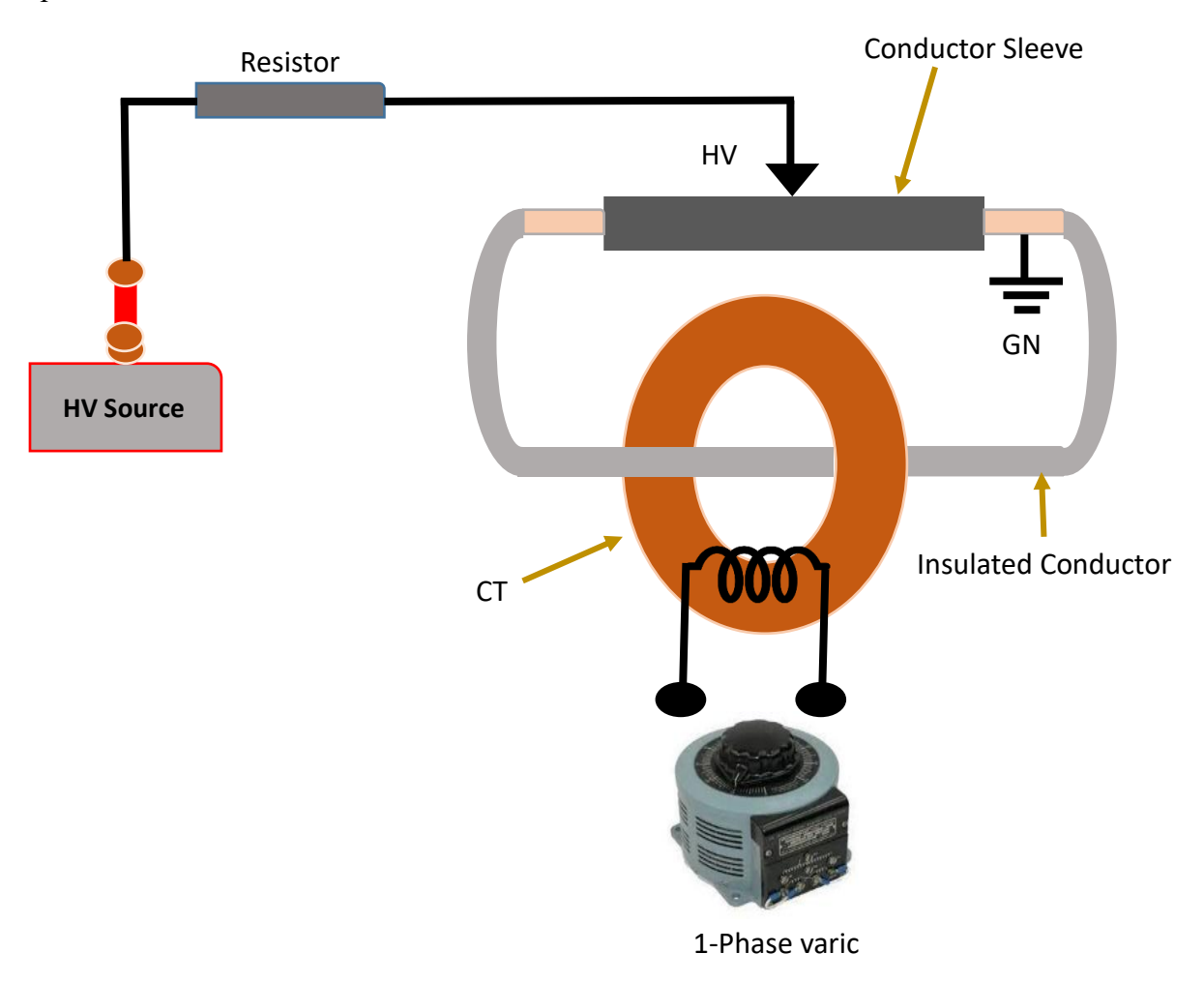


Figure 5.1 Schematic representation of experimental setup for electrical tracking phenomena under varying loading conditions.



Figure 5.2 Experimental setup for electrical tracking phenomena under varying loading conditions.

The setup employs a current transformer (CT) whose primary is connected through a singlephase variac to regulate the input current. An insulated conductor is placed, passing through the air gap between the primary & the ferromagnetic core of the CT.

TABLE 5.1

Load current & thermal Effects on conductor sleeve performance without insulation tape

Sl. No.	Temperature	Load current on CC	ITIVexp
	(K)	(A)	(kV)
1	303.15	58	28.2
2	313.15	84	25.35
3	323.15	110	24.1
4	343.15	130	24.1
5	363.15	153	24.1

The results obtained from these tests are presented in table 5.1, which illustrates the observed trends and behaviors of CS under varying load currents and temperatures. It is evident from the results that an increase in load current (from 58 A to 153 A) leads to a rise in conductor temperature (from 303.15 K to 363.15 K), as expected due to Joule heating. This rise in

temperature initially results in a significant reduction in the tracking inception voltage (ITIV_{exp}), which dropped from 28.2 kV at 303.15 K to 24.1 kV at 323.15 K. This reduction is likely due to thermal aging of the silicone rubber, which degrades its dielectric properties and reduces its hydrophobicity, making the surface more prone to tracking under electrical stress.

However, beyond 343.15 K, ITIV_{exp} stabilizes at 24.1 kV, even as the temperature and load current increase further to 363.15 K and 153 A, respectively. This suggests that the silicone rubber reaches a thermal limit where its dielectric properties no longer degrade significantly, possibly due to the material entering a stable degraded state (e.g., complete loss of hydrophobicity or saturation of thermal degradation effects). These findings provide valuable insights into the relationship between load current, thermal stress, and the performance of CS under operational conditions. They indicate that CS may have a temperature threshold (around 343.15 K) beyond which their ability to resist tracking does not degrade further, which is critical for determining safe operating limits in high-voltage applications. This understanding can guide the design and selection of insulating materials for conductors, ensuring reliability under varying thermal and electrical stresses.

5.2 CS with insulation tape:

As shown previously, the interfacial region plays a critical role in electrical tracking and runaway phenomena, thus, in an attempt to increase the ITIV, an additional insulation tape is applied on the outer tip of interfacial region as shown in figure 5.2, and the corresponding schematics of figure 5.3 respectively. Further, similar experiments as in previous section (5.1) were performed.



Figure 5.3 Conductor sleeve when insulation tape applied on the outer tip of interfacial region.

Further, a comparative analysis was conducted to evaluate the effect of insulation tape. The schematic of experimental setup is shown in figures 5.3. In this study, CS were tested under identical loading and thermal conditions same as previous section (5.1), to ensure consistency in the evaluation process. The comparison between table 5.1 (without insulation tape) and table 5.2 (with insulation tape) is plotted in figure 5.4, demonstrates that the addition of insulation tape to silicone rubber conductor sleeves significantly enhances their tracking resistance under thermal and electrical stress. While the temperature and load current trends remain identical in both setups (rising from 303.15 K at 58 A to 363.15 K at 153 A), the ITIV_{exp} values are consistently higher with the insulation tape, with increases ranging from 1.2 kV to 2.05 kV (5.0% to 7.9%) across all test conditions.

TABLE 5.2

Load current & thermal effects on conductor sleeve performance with insulation tape

Sl. No.	Temperature	Load current on CC	ITIVexp
	(K)	(A)	(kV)
1	303.15	58	30.25
2	313.15	84	27.35
3	323.15	110	25.4
4	343.15	130	25.4
5	363.15	153	25.4

Additionally, the ITIV_{exp} stabilizes at the same temperature point in both setups (at 343.15 K), with values of 25.4 kV with the insulation tape (table 5.2) compared to 24.1 kV without the tape (table 5.1). This improvement in ITIV_{exp} with the tape indicates that the insulation tape enhances the dielectric performance of the insulating system, despite reaching thermal saturation at the same temperature. The higher ITIV_{exp} suggests that the insulation tape acts as an effective dielectric barrier, reducing electrical stress on the silicone rubber surface and improving resistance to tracking, likely by providing additional insulation and surface protection. These findings highlight the value of using insulation tape in high-voltage applications to enhance the performance and reliability of silicone rubber conductor sleeves, particularly under elevated temperatures. Engineers can leverage this tape to improve the

tracking resistance of such sleeves, ensuring better safety and performance in practical scenarios.

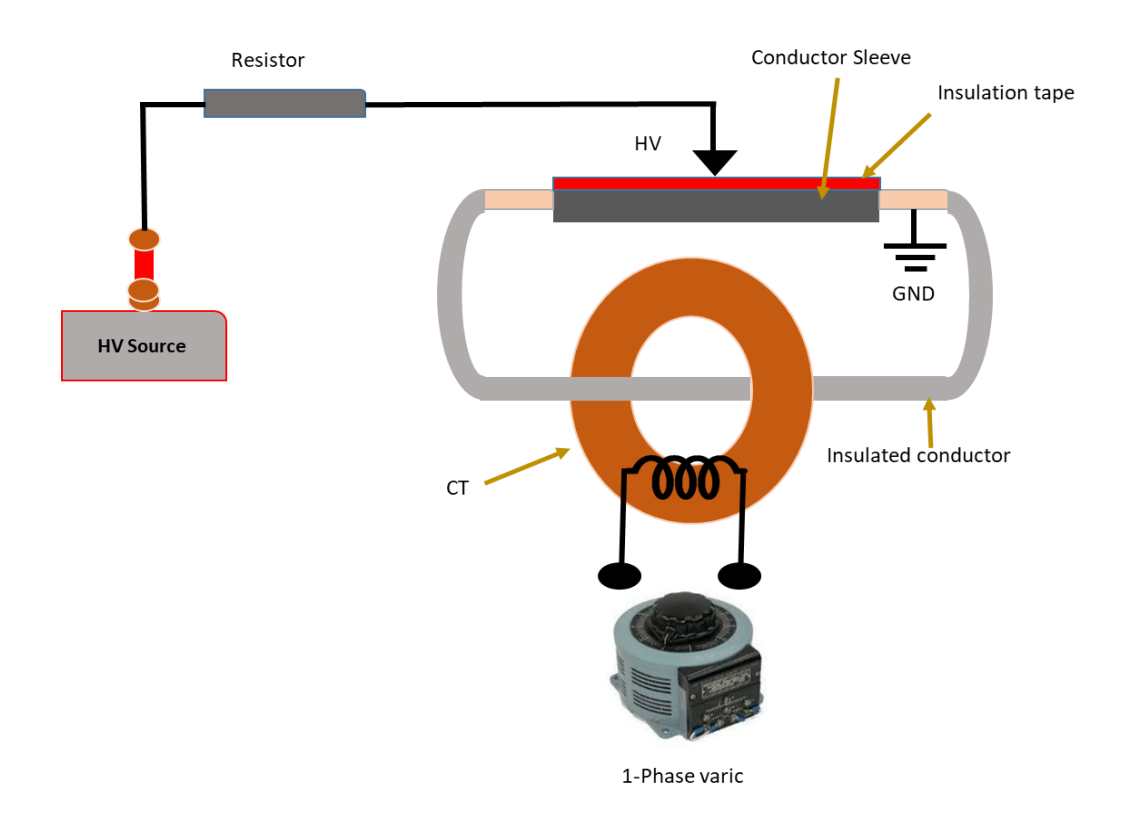


Figure 5.4 Schematic representation of experimental setup for electrical tracking phenomena under varying loading conditions with insulation tape.

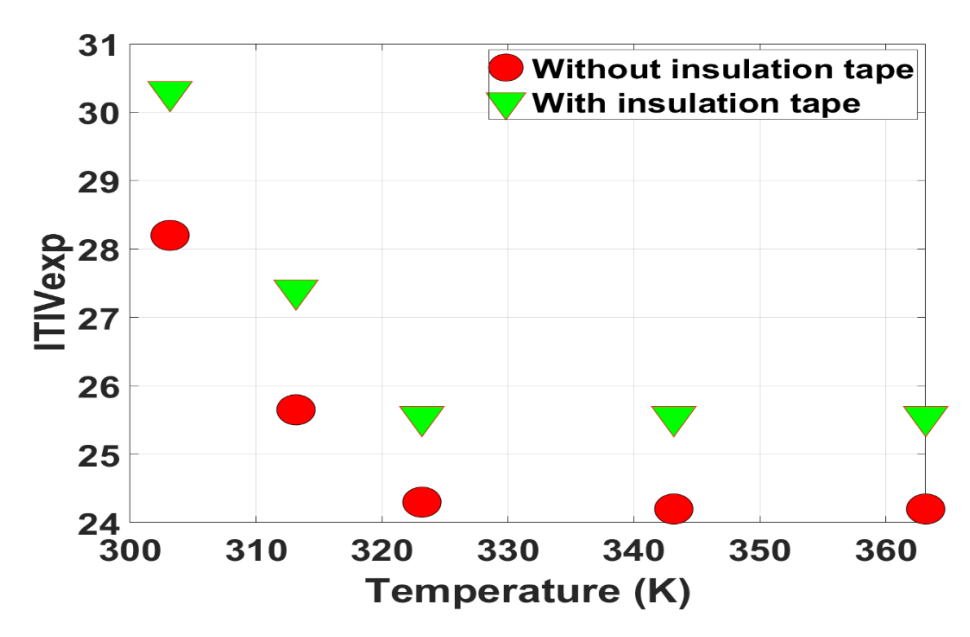


Figure 5.5 Experimentally obtained interfacial tracking inception voltage with and without insulation tape

5.3 FEM-based analysis of load current effects on runaway phenomenon

The results discussed in the previous chapter were primarily based on no-load conditions, where the runaway phenomenon is predominantly caused by the intrinsic dielectric heating of the insulation material. Previous studies have shown that runaway can be initiated at any temperature, including those close to ambient levels, though higher initial temperatures tend to accelerate the instability process [37-38].

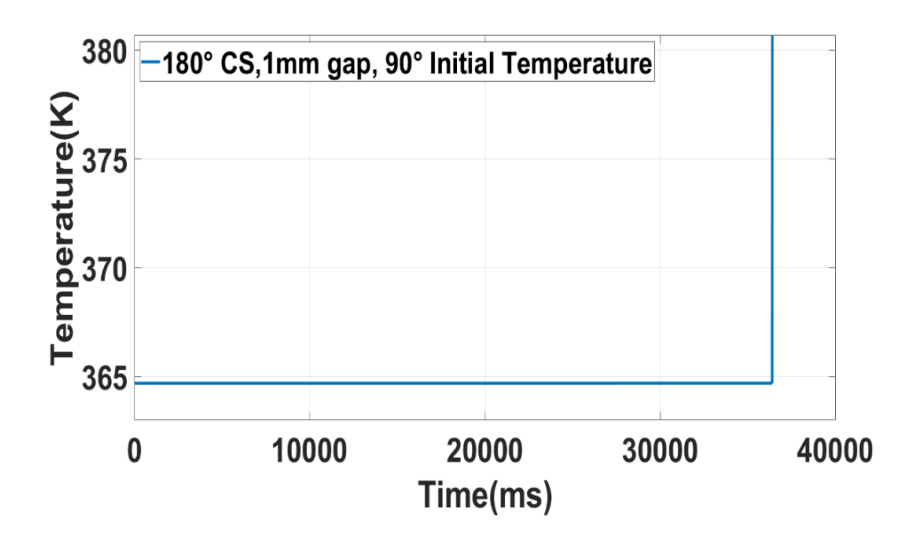


Figure 5.6 Runaway characteristics in the interface region for 180° (90° initial temperature) overlapped CS.

To investigate the effect of load current on the performance of conductor sleeves without insulation tape, a specific scenario was analysed using finite element method (FEM) simulations. The study focused on a 180° conductor sleeve (CS) with a tree branch acting as a ground electrode, positioned 1 mm away from the CS surface. In this setup, load current was introduced into the FEM simulation to stabilize the conductor temperature at 363.15K(90°C), reflecting realistic operating conditions. After achieving steady-state thermal conditions, a time-domain simulation was performed to examine the instability mechanism and its progression.

The results, illustrated in figure 5.5, reveal that under loaded conditions, the runaway phenomenon was triggered at a significantly lower voltage of 15 kV compared to the 43.3 kV observed under no-load conditions for the same 1 mm gap, as previously reported in table 4.3. This indicate that load current not only reduces the threshold voltage for runaway but also significantly alters the thermal-electrical dynamics of the system. This reduction in

runaway voltage attributed to the additional thermal stress induced by the load current, which exacerbates the dielectric heating and accelerates the onset of instability.

These findings highlight the combined effects of load current and thermal stress on the performance of conductor sleeves under real-world conditions. They emphasize the critical importance of considering load-induced thermal dynamics in the design and evaluation of conductor sleeve systems to ensure reliability and safety in power transmission networks. This study underscores the need for advanced modelling and testing approaches to account for such factors in practical applications.

5.4 Conclusions

This chapter investigates the impact of load current on CS performance, focusing on thermal and electrical stresses. Experimental results show that increasing load current raises conductor temperature, reducing ITIV due to thermal aging of silicone rubber, with stabilization at 343.15 K. Applying insulation tape at the interfacial region increases ITIV by 5.0% to 7.9%, enhancing tracking resistance. FEM simulations under loaded conditions reveal a lower runaway voltage (15 kV vs. 43.3 kV no-load) for 180° CS, highlighting the role of load-induced thermal stress in accelerating instability. These findings emphasize the need to consider load current in CS design to ensure reliability under operational conditions.

Conclusions and Future Work

6.1 Conclusions

This thesis provides a comprehensive evaluation of the design of overhead conductor sleeves (CS) with a specific focus on interfacial tracking and runaway phenomena. Based on experimental and simulation results, the following detailed conclusions have been drawn

I. Initiation of Tracking and Runaway

The interface of conductor sleeves (CS) is identified as the most susceptible region for the initiation of tracking and runaway. This is attributed to the higher conductivity at the interface, which promotes localized heating and enhances the likelihood of surface degradation, leading to the formation of conductive paths and subsequent arc initiation.

II. Comparison of Overlap Configurations

The experimental and simulated inception tracking voltages (ITIV) for the 90° overlapped CS configuration are observed to be significantly lower than those of the 180° overlapped design. This indicates that the 180° overlap provides superior resistance to tracking and runaway, making it a more robust choice for high-performance applications.

III. Performance Enhancement for 90° Overlapped CS

To improve the dielectric performance of the 90° overlapped CS and bring its ITIV values closer to those of the 180° configuration, the insulation thickness can be increased. This modification would enhance the electrical integrity of the 90° CS, reducing the risk of tracking and improving overall reliability.

IV. Comparison Between CS and CC

The 180° overlapped CS is found to outperform CCs in terms of electro-thermal performance, making it a more suitable alternative to replace overhead bare conductors (OBC). Additionally, the 180° CS design offers practical advantages, including greater flexibility during installation and easier handling in operational environments, further solidifying its position as the preferred choice in medium-voltage transmission systems.

These findings underscore the importance of optimizing sleeve designs to improve performance and operational reliability while addressing the practical challenges associated with modern power systems.

V. Impact of Load Current on CS

The study highlights the significant impact of load current on the performance and reliability of conductor sleeves, emphasizing that increased load currents lead to higher temperatures, material degradation, and earlier breakdowns. The application of insulation tape proves effective in improving the dielectric strength and delaying tracking phenomena. These findings underscore the importance of considering load-induced thermal and electrical stresses in the design and evaluation of conductor sleeves to ensure their longevity and safe operation in power transmission systems.

6.2 Future work

Future research should focus on conducting long-term accelerated aging tests to gain a deeper understanding of the degradation mechanisms of conductor sleeves under various environmental and operational conditions, including high temperature, moisture, and mechanical wear. Additionally, exploring advanced insulation methods, such as multi-layer or nanocoating's, could further enhance the dielectric strength of conductor sleeves and prevent tracking and runaway phenomena under different stress conditions.

Another important area of investigation is the optimization of the overlapping area in conductor sleeves. While an increase in the overlapping area improves the interfacial tracking inception voltage (ITIV), it introduces challenges such as increased weight, sag, and heat dissipation. Furthermore, larger overlapping areas make it more difficult to wrap the conductor sleeve around the bare conductor effectively. Therefore, it is essential to explore optimal solutions that maintain the same overlapping angle while extending the tracking path, which will enhance tracking performance and improve breakdown resistance.

By addressing these areas in future research, we aim to provide a comprehensive understanding of the impact of load current and overlapping area on conductor sleeve performance, ultimately contributing to the development of more efficient and effective designs.

References

- [1] D. T. Eccleston, J. F. Dwyer, R. E. Harness, T. A. Barnes, and J. Downie, "Wildfire risk reduction through wildlife risk mitigation," *in Proc. IEEE Rural Electric Power Conf.* (REPC), Cleveland, OH, USA, 2023, pp. 32–38, doi: 10.1109/REPC49397.2023.00014.
- [2] K. Alstad, S. Refsnaes, T. Bovre, and H. Thomassen, "A new overhead line concept based on covered conductors," *in Proc. 12th Int. Conf. Electricity Distribution (CIRED)*, Birmingham, UK, 1993, pp. 3.7/1–3.7/5, vol. 3.
- [3] E. Rimkus, E. Stonevičius, I. Gečaitė, V. Mačiulytė, and D. Valiukas, "Impact of meteorological conditions on overhead transmission line outages in Lithuania," *Atmosphere*, vol. 15, no. 11, p. 1349, Nov. 2024, doi: 10.3390/atmos15111349.
- [4] J. Pihler and I. Ticar, "Design of systems of covered overhead conductors by means of electric field calculation," *IEEE Trans. Power Del.*, vol. 20, no. 2, pp. 807–814, Apr. 2005, doi: 10.1109/TPWRD.2004.839210.
- [5] A. J. Thomas, I. C, and C. C. Reddy, "A method for surface voltage measurement of an overhead insulated conductor," *IEEE Trans. Instrum. Meas.*, vol. 70, pp. 1–8, 2021, Art no. 6000708, doi: 10.1109/TIM.2020.3021803.
- [6] R. Fernandes da Silva and V. S. Filho, "Analysis of electrical tracking by energy absorption during surface discharge in polymeric materials," *IEEE Trans. Dielectr. Electr. Insul.*, vol. 23, no. 1, pp. 501–506, Feb. 2016, doi: 10.1109/TDEI.2015.005002.
- [7] A. Syakur, H. Berahim, I. Tumiran, and R. Rochmadi, "Electrical tracking formation on silane epoxy resin under various contaminants," *Telkomnika*, vol. 11, no. 1, pp. 17–28, Jan. 2013.
- [8] N. Yoshimura, S. Kumagai, and B. Du, "Research in Japan on the tracking phenomenon of electrical insulating materials," *IEEE Electr. Insul. Mag.*, vol. 13, no. 5, pp. 8–19, Sep./Oct. 1997.
- [9] J. Y. Li, C. X. Sun, and S. A. Sebo, "Humidity and contamination severity impact on the leakage currents of porcelain insulators," *IET Gener. Transm. Distrib.*, vol. 5, no. 1, pp. 19–28, Jan. 2011.

- [10] N. A. M. Jamil, M. A. M. Piah, F. L. Muhamed, N. F. Kasri, N. A. Muhamad, and Q. E. Kamarudin, "Electrical tracking characterization of LLDPE-natural rubber blends filled with nanofillers," *in Proc. IEEE Conf. Electr. Insul. Dielectr. Phenomena (CEIDP)*, Shenzhen, China, 2013, pp. 695–698.
- [11] A. Syakur, H. Berahim, I. Tumiran, and R. Rochmadi, "Experimental investigation on electrical tracking of epoxy resin compound with silicon rubber," *Gaodianya Jishu/High Voltage Eng.*, vol. 37, no. 11, pp. 2780–2785, Nov. 2011.
- [12] B. X. Du and M. Xiao, "Effects of thermally conducting particles on resistance to tracking failure of polyimide/BN composites," *IEEE Trans. Dielectr. Electr. Insul.*, vol. 21, no. 4, pp. 1565–1572, Aug. 2014.
- [13] G. C. da Silva et al., "Different configurations of spacer cable system under multiple stress tests," in *Proc. IEEE/PES Transm. Distrib. Conf. Expo. (T&D)*, Dallas, TX, USA, 2016, pp. 1–5, doi: 10.1109/TDC.2016.7520046.
- [14] ASTM International, "Standard test method for dust-and-fog tracking and erosion resistance of electrical insulating materials," *ASTM* D2132-01, 2001.
- [15] ASTM International, "Electrical insulating materials," ASTM D1376-00, 2000.
- [16] International Electrotechnical Commission, "Method for the determination of the proof and the comparative tracking indices of solid insulating materials," *IEC* 60112, 2003.
- [17] Electrical insulating materials used under severe ambient conditions, "test methods for evaluating resistance to tracking and erosion" *IEC* 60587, 2022.
- [18] Arshad, G. Momen, M. Farzaneh, and A. Nekahi, "Properties and applications of superhydrophobic coatings in high voltage outdoor insulation: A review," *IEEE Trans. Dielectr. Electr. Insul.*, vol. 24, no. 6, pp. 3630–3646, Dec. 2017, doi: 10.1109/TDEI.2017.006725.
- [19] M. Ullah, M. Amin, H. Hussain, and M. T. Nazir, "Impact of accelerated ultraviolet weathering on polymeric composite insulators under high voltage DC stress," *CSEE J. Power Energy Syst.*, vol. 8, no. 3, pp. 922–932, May 2022, doi: 10.17775/CSEEJPES.2020.01900.

- [20] D. Ghose and D. Khastgir, "Degradation and stability of polymeric high voltage insulators and prediction of their service life through environmental and accelerated aging process," *ACM Trans. Mater. Res.*, vol. 3, no. 9, Sep. 2018.
- [21] O. Kabot, J. Fulneček, S. Mišák, L. Prokop, and J. Vaculík, "Partial discharges pattern analysis of various covered conductors," in *Proc. 21st Int. Sci. Conf. Electric Power Eng.* (*EPE*), Prague, Czech Republic, 2020, pp. 1–5, doi: 10.1109/EPE51172.2020.9269171.
- [22] S. Mišák, J. Fulneček, T. Vantuch, T. Buriánek, and T. Jezowicz, "A complex classification approach of partial discharges from covered conductors in real environment," *IEEE Trans. Dielectr. Electr. Insul.*, vol. 24, no. 2, pp. 1097–1104, Apr. 2017, doi: 10.1109/TDEI.2017.006135.
- [23] L. Zhou, Y. Tian, W. Chen, S. Huang, and T. Wen, "Characteristics of partial discharge on 10 kV covered conductor around tower head," *IEEE Access*, vol. 10, pp. 98140–98152, Sep. 2022, doi: 10.1109/ACCESS.2022.3206374.
- [24] Y. Yan, Y. Zhao, W. He, I. S. Stievano, and H. Li, "On-line partial discharge localization of 10-kV covered conductor lines," *IEEE Trans. Power Del.*, vol. 38, no. 3, pp. 1688–1698, Jun. 2023, doi: 10.1109/TPWRD.2022.3221010.
- [25] IEEE Power and Energy Society, "IEEE guide for protective relay applications to transmission lines," *IEEE Std* C37.113-2015, Jun. 2016, doi: 10.1109/IEEESTD.2016.7502047.
- [26] O. Kabot, L. Klein, L. Prokop, and W. Walendziuk, "Enhanced fault type detection in covered conductors using a stacked ensemble and novel algorithm combination," *Sensors*, vol. 23, no. 20, p. 8353, Oct. 2023, doi: 10.3390/s23208353.
- [27] J. Fulneček and S. Mišák, "A simple method for tree fall detection on medium voltage overhead lines with covered conductors," *IEEE Trans. Power Del.*, vol. 36, no. 3, pp. 1411–1417, Jun. 2021, doi: 10.1109/TPWRD.2020.3008482.
- [28] O. Kabot, L. Klein, L. Prokop, and W. Walendziuk, "Dataset for antenna-based detection of fault types in covered conductors for 22 kV voltage power lines," *Sci. Data*, vol. 11, p. 1319, Dec. 2024, doi: 10.1038/s41597-024-04009-1.

- [29] Gala Thermo Shrink PVT. LTD. "Overhead Line Cover Silicone Self-locking." https://www.galathermo.com/heat_shrink_end_caps/cable_end_sealing_caps/Overhead_Line Cover Silicone Self locking.html
- [30] P. Johri, C. C. Reddy and C. Kumar, "Electric Field Dynamics in PILC Side of dry Type MV Heat-Shrink Transition Joints" in *IEEE Transactions on Power Delivery*, vol. 37, no. 3, pp. 1888-1896, June 2022, doi: 10.1109/TPWRD.2021.3099861.
- [31] J. M. Oudin and H. Thevenon, "DC cables determination of the gradient actually applied to the insulant and its experimental correlation with breakdown gradient," in *CIGRE*, Paris, France, 1966, paper 208.
- [32] C. C. Reddy and T. S. Ramu, "On the intrinsic thermal stability in HVDC cables," *IEEE Trans. Dielectr. Electr. Insul.*, vol. 14, no. 6, pp. 1509–1515, Dec. 2007, doi: 10.1109/TDEI.2007.4401235.
- [33] ASTM International, "Standard test methods for DC resistance or conductance of insulating materials," *ASTM* D257-07, Jul. 2012.
- [34] ASTM International, "Standard test method for AC loss characteristics and permittivity of solid electrical insulation," *ASTM* D150-98, Mar. 1999.
- [35] A. Heras, "Can Maxwell's equations be obtained from the continuity equation?" *Amer. J. Phys.*, vol. 75, no. 7, pp. 652–657, Jul. 2007.
- [36] S. Dhayalan and C. C. Reddy, "Simulation of electro-thermal runaway and thermal limits of a loaded HVDC cable," *IEEE Trans. Power Del.*, vol. 37, no. 4, pp. 2621–2628, Aug. 2022, doi: 10.1109/TPWRD.2021.3112558.
- [37] C. Iyyappan and C. C. Reddy, "Inverse power law based inclusive life model for DC polarity reversal stresses," *IEEE Trans. Dielectr. Electr. Insul.*, vol. 28, no. 2, pp. 586–593, Apr. 2021, doi: 10.1109/TDEI.2020.009281.
- [38] G. Mazzanti, "The combination of electro-thermal stress, load cycling and thermal transients and its effects on the life of high voltage AC cables," *IEEE Trans. Dielectr. Electr. Insul.*, vol. 16, no. 4, pp. 1168–1179, Aug. 2009, doi: 10.1109/TDEI.2009.5211872.